



LCL FILTER PARAMETER ESTIMATION FOR A GRID-CONNECTED PWM SWITCHED VOLTAGE SOURCE INVERTER

Lappeenranta-Lahti University of Technology LUT

Master's Program in Computational Engineering, Master's Thesis

2024

Tommi Kankaanranta

Examiners: Professor Lassi Roininen
 Professor Pasi Peltoniemi

ABSTRACT

Lappeenranta-Lahti University of Technology LUT
School of Engineering Science
Computational Engineering

Tommi Kankaanranta

LCL Filter Parameter Estimation for a Grid-Connected PWM Switched Voltage Source Inverter

Master's thesis

2024

52 pages, 10 figures, 11 tables, 1 appendix

Examiners: Professor Lassi Roininen and Professor Pasi Peltoniemi

Keywords: differential evolution, Fast Fourier Transform, optimization, PWM modulation, parameter estimation

The motivation for this study was induced by a practical electrical industry problem of coupling a square-wave switched power converter to the electrical grid. This arrangement requires a conditioning element to meet industry and regulatory standards for grid-connected devices. To this end, the main research question of this study was to investigate whether or not differential evolution global optimisation method could be utilised to identify the design parameters of the conditioning element. The three stages of the conditioning element are: inductance L , capacitance C , and inductance L . Combining these the LCL filter topology is formed. The objectives of this work were to construct respective models and simulation environment to simulate the behaviour of the system. Differential evolution was utilised to derive new LCL design parameter candidates for computing and comparing the performance characteristics of the solution with respect to the set performance targets. Three increasing number of generations of differential evolution process were studied, where the top three LCL design parameter candidates of each generation size were investigated more closely. The differential evolution optimisation process exhibited convergence as the generation sizes increased. The produced LCL design parameter candidates tended to the set performance characteristics targets. Consequently, the proposed method of the study produced meaningful results that are worth exploring either in industrial or academic setting further.

TIIVISTELMÄ

Lappeenrannan-Lahden teknillinen yliopisto LUT
Insinööritieteiden tiedekunta
Laskennallinen tekniikka

Tommi Kankaanranta

PWM ohjatun ja verkkoon kytketyn tehonmuokkaimen LCL suotimen suunnittelu- parametrien etsiminen

Diplomityö

2024

52 sivua, 10 kuvaa, 11 taulukkoa, 1 liite

Tarkastajat: Professori Lassi Roininen ja Professori Pasi Peltoniemi

Hakusanat: differentiaalievoluutio, nopea Fourier-muunnos, optimointi, PWM modulaatio, parametrien etsiminen

Tutkimusaihe syntyi valmistavanteollisuuden käytännönongelmasta kytkeä kanttiaalto-ohjattuja tehonmuokkaimia sähköverkkoon. Sähköverkkoon kytkettäviin laitteisiin liittyy vahvasti teollisuusstandardit ja viranomaissäädökset, kuten laitteiden häiriönsieto tai niiden tuottamat sähkö-magneettiset häiriöt. Näihin laadullisiin kriteereihin pääsemiseksi tarvitaan tehonmuokkaimen pariin suotimia, kuten LCL suodin. Kyseinen suodin koostuu kolmesta erillisestä vaiheesta, jossa L viittaa induktanssiin, C kapasitanssiin, ja L induktanssi suotimen viimeisenä vaiheena sen rakenteessa. Tämän työn päätutkimuskysymys olikin, että voidaanko differentiaalievoluutio optimointimenetelmää soveltaa etsimään LCL suotimen arvot niin, että ne täyttäisivät sen ja tehonmuokkaimen yhdessä muodostamalle järjestelmälle ennalta-asetetut laadulliset kriteerit. Tätä varten tutkimuksessa oli luotava matemaattiset mallit ja simulointiympäristö, jonka puitteissa LCL suodinkandidaatteja voitiin arvioida niiden tuottamaan laadulliseen vasteeseen. Tätä arvioitiin kolmella eri differentiaalievoluutio generaatiokoolla, joista kunkin generaatiomäärän kolme parhaita ratkaisua poimittiin lähempään tarkasteluun. Osoittautui, että differentiaalievoluution tuottamat ratkaisut suppenivat kohti haluttuja laadullisia kriteereitä kun generaatioiden koko kasvoi. Tulosten perusteella työssä kehitetty menetelmä tuotti tuloksia, joita on mahdollista hyödyntää ja jatkokehittää, joko teollisen tai akateemisen jatkotutkimuksen puitteissa.

ACKNOWLEDGEMENTS

I would like to thank both of my supervisors, Professor Lassi Roininen and Professor Pasi Peltoniemi, for providing the support, constructive discussions, and patience. As this study was conducted in parallel with a regular day job it proved valuable to know that they were at disposal to share their insights. Other valuable source of support were my longstanding colleagues Antti Tarkiainen and Matti Iskanius, what they might have considered as casual conversations at work, proved to be very important input to carry on with the work. This gave confidence to the author for being in the right path. Finally, this work would surely not have realised without the support and patience of the family, where my wife Henriika with my two sons Nikke and Emil had to bear the often absentminded husband and father.

Lappeenranta, November 25, 2024

Tommi Kankaanranta

LIST OF ABBREVIATIONS

AC	Alternating Current
DC	Direct Current
DE	Differential Evolution
EHD	Extended Harmonic Domain
EMC	Electro-Magnetic Compatibility
ES	Evolution Strategies
FE	Forward-Euler
FFT	Fast Fourier Transform
GA	Genetic Algorithm
GPU	Graphics Processing Unit
HVDC	High Voltage Direct Current
LCL	Inductance L , Capacitance C , Inductance L
LSQ	Least Squares
LTI	Linear Time Invariant
LTP	Linear Time Periodic
NLSQ	Nonlinear Least Squares
ODE	Ordinary Differential Equation
PF	Power Factor
PI	Proportional-Integral
PWM	Pulse Width Modulation
RK	Runge-Kutta
RMS	Root-Mean-Square
SA	Simulated Annealing
SPWM	Sinusoidal Pulse Width Modulation
SVM	Space Vector Modulation
TDD	Total Demand Distortion
THD	Total Harmonic Distortion
VSI	Voltage Source Inverter

LIST OF SYMBOLS

C_f	Filter capacitance
E_{tot}	Instantaneous total energy stored in the filter
F_{obj}	Objective function
L_f	Filter inductance
L_g	Grid-side inductance
L_i	VSI-side inductance
P	Active power
P_g	Grid-side active power
Q	Reactive power
R_d	Damping resistance
R_g	Grid-side resistance
R_i	VSI-side resistance
T_0	Fundamental wave period length
$\Omega[\mathbf{x}^L, \mathbf{x}^U]$	Solution search space
PF_g	Grid-side power factor
THD_{i_g}	THD of the current i_g
THD_{i_i}	THD of the current i_i
$\text{THD}_{u_{C_f}}$	THD of the voltage u_{C_f}
$\mathbf{x}^{(0)}$	Initial state-vector
$\mathbf{x}^{(k)}$	k^{th} iteration state-vector
\mathbf{x}^L	Lower bound of the search space
\mathbf{x}^U	Upper bound of the search space
\mathbf{p}_{est}	Estimated system performance characteristics
\mathbf{p}_{ref}	Reference system performance characteristics
θ_0	Fundamental wave phase-shift
θ_c	Carrier wave phase-shift
f_g	Fundamental frequency of the grid
f_{res}	Resonance frequency
f_{sw}	PWM switching frequency of the carrier
i_g	Grid-side current
i_i	VSI-side current
m_a	SPWM modulation amplitude
u_{C_f}	Filter capacitor voltage
u_{dc}	DC voltage
u_g	Grid-side voltage
u_i	VSI-side voltage

CONTENTS

1	INTRODUCTION	8
2	RELATED WORK	11
2.1	Iterative	11
2.2	Optimisation	17
3	PROPOSED METHODS	22
3.1	VSI-model	22
3.2	LCL-model	27
3.3	Performance characteristics	30
3.4	Differential evolution optimisation	31
4	EXPERIMENTS	34
4.1	Environment and models	34
4.2	Characteristics	38
4.3	Objective function	38
4.4	Solution candidates	40
5	DISCUSSION AND CONCLUSIONS	46
	REFERENCES	49
	APPENDICES	

Appendix 1: Additional results from the experiments.

1 INTRODUCTION

The rise of renewable energy production has paved the way for utility grid-connected energy sources, such as: wind power, photovoltaic, and hydrogen fuel cell based ones [1–5]. Many modern Voltage Source Inverter (VSI) devices are Pulse Width Modulation (PWM) controlled providing a square wave phase Direct Current (DC) output [1, 6]. Thus, for any practical end-user applications the DC output needs to be conditioned to Alternating Current (AC) output [1, 5, 6]. More often than not the VSI is connected to the utility grid through a conditioning element, such as: Inductance L , Capacitance C , Inductance L (LCL) filter [1–6]. An example of such grid-connected application is depicted in Figure 1.

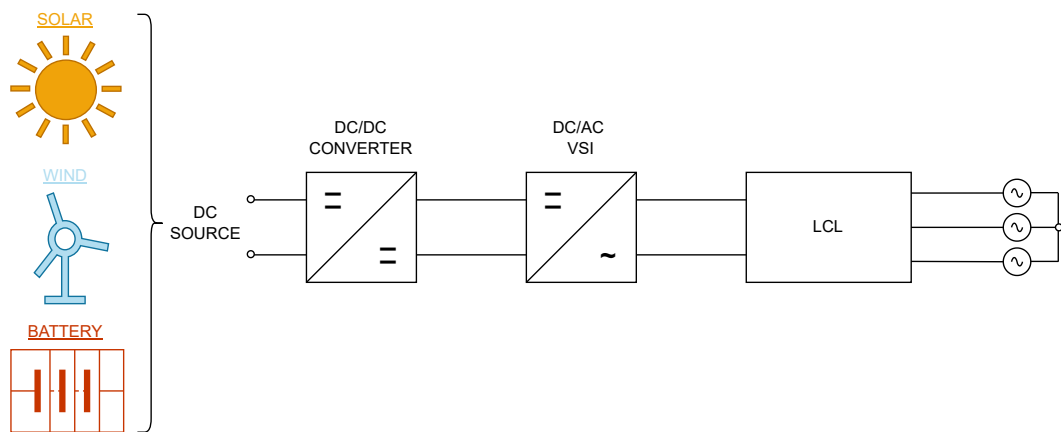


Figure 1. A typical VSI and LCL filter setup in a grid-connected application adapted from Reznik *et al.* [1].

There are a number reasons for doing this kind of conditioning, but whatever the solution, it needs to be compliant with applicable regulatory and industry standards. Such driving factors, for example, are grid code specifications [7] for High Voltage Direct Current (HVDC) systems and electric quality standards [8, 9] for grid-connected applications. There can also be additional application specific requirements involved, such as Electro-Magnetic Compatibility (EMC) standards, of which IEC 60533 [10] and IEC 62040-2 [11] for island grid applications to give as an example. Ultimately the solution needs to cover the technical and regulatory requirements, but also be cost effective, which has lead the industry to adopt LCL filters as a practical choice for grid-connected applications when coupled with a VSI [1–6, 12].

Considering the setting and background of this thesis work, it is apparent that the chosen topic is multidisciplinary, where mathematical models and methods are being applied to a practical electrical engineering design research question. Consequently, the main research question is, simply, that: can Differential Evolution (DE) global optimisation method be applied to identify the design parameters of the chosen LCL filter topology? While the main research question can be characterized as straightforward, it can be subdivided into several sub-objectives. Thus, in a finer level of detail, the objectives for this thesis work are as follows:

1. Development of a mathematical model describing the behaviour of a PWM switched VSI.
2. Development of a mathematical model describing the behaviour of a LCL filter.
3. Identification of the performance characteristics of a candidate solution.
4. Applicability of the DE global optimisation method in identifying candidate solutions.
5. Construction of a simulation environment with the aforementioned models and optimisation method.
6. Finally, evaluation of the feasibility of the DE candidate solutions with respect to the performance metrics.

For this work to have a reasonable scope, emphasis will be placed on the mathematical modelling and the respective parameter identification methods, rather than the underlying physics. Consequently, the following delimitations on the scope of this work shall be placed:

- Mathematical methods over detailed treatment of the underlying physics.
- Focus on DE global optimisation method in the described setting.
- Finally, evaluation of the developed concept and its viability over production deployment.

It is therefore, a conscious decision of the author to choose emphasis on mathematical models over developing physics based ones, such as for the VSI or the LCL filter. Here, the author also chooses to rely on existing literature and research in the field rather. The motivation is to give more space for the treatment of the mathematical methods, such as

DE, being applied to the underlying practical engineering problem which in this case is coming from the field of electrical engineering. However, this should not detract from the viability of the proposed method being in the described real world setting. This may require additional research and development further, but is judged by the author to be outside of the scope of this work.

It is also worth pointing out the topology of the grid-connected VSI and LCL filter system that shall be used and analysed in this work from Section 3 onward. Namely, the selected layout of the filter capacitors C_f and the serial damping resistors R_d , where the wye-connected configuration shall only be considered – not delta-connected. Finally, the PWM scheme shall be fixed to Sinusoidal Pulse Width Modulation (SPWM). In Figure 2 there is a diagram of the system, that has been adapted from the several references used in the scope of this work [1–6, 12]. Given the rich variability in, both, the system to be modelled and the proposed solutions the author of this work judged appropriate standardize the grid-connected system under evaluation. For the purpose of this work, the system that shall be here onward considered is depicted in Figure 2, which is motivated by Reznik *et al.* [1].

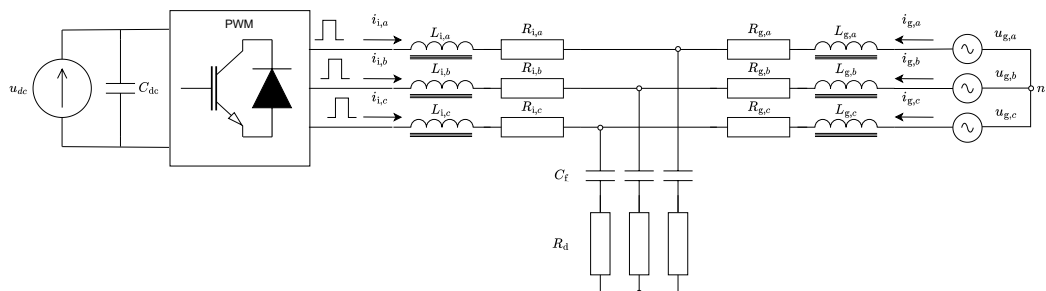


Figure 2. Adapted and standardized grid-connected system with VSI and LCL in the scope of this work.

Apart from the introduction, scope, and objectives of this work presented in this section the work is organized into subsequent four sections. Section 2 explores prior work in the field and introduces the necessary theoretical background for this work. Followed by Section 3, where the proposed methods of this work shall be introduced. All developed algorithms, mathematical models, or tools will be presented here. Continuing to Section 4, which describes the experiments derived from the respective methods introduced in Section 3. Finally, in Section 5 the results of the experiments conducted in Section 4 are being discussed and the conclusions of the work are drawn out with improvement and development ideas for the future.

2 RELATED WORK

The field of electrical engineering is rich in research papers exploring the problem of identifying design parameters of a LCL filter coupled with a grid-connected VSI [1–6,12]. Several alternative design procedures have been proposed by the researchers, where many of them are addressing specific and predetermined performance characteristics with respect to some design constraints. These design procedures can be categorized based on the solution approach taken [4,5]. Namely, the two predominant approaches are: iterative and optimisation based. In the iterative approach, the LCL filter designer is following a step-by-step procedure, where in each step the effect of the respective design parameters are evaluated until desired design objective is satisfied [6]. Conversely, the optimisation of analytical expressions procedure requires identifying a mathematical model that captures the relevant design parameters with respect to predetermined performance characteristics, where the expression is subject to one or several constraints [5]. Given the great degree of freedom in implementing either iterative or optimising design procedure – dedicated sections, Section 2.1 and Section 2.2, are used to explore the respective approaches in finer detail.

2.1 Iterative

In the paper by Liserre *et al.* [6] the authors propose a step-by-step design procedure, which consists of implementing closed-loop controllers for the VSI with iterative identification of the respective LCL filter design parameters. The goal of the DC-side voltage and VSI-side AC current Proportional-Integral (PI) controllers is to improve the dynamic performance of the system. The iterative LCL filter design parameter identification process attempts to decrease the switching ripple induced by the VSI's PWM switching, such that the amount of filter hardware required to meet the predetermined performance characteristics is minimized. More specifically, the LCL filter aims in the reduction of the grid side high-order current harmonics, such that a desired level of attenuation and mitigation of the oscillation effects are achieved. This leads to the conclusion, that in a single-phase equivalent of the LCL filter in Figure 2, the L_i and L_g should be carefully chosen in terms of the LCL filter's current ripple and damping characteristics.

Consequently, the process of identifying the LCL filter design parameters in the paper by Liserre *et al.* [6] starts by defining the inputs and constraints of the procedure. For the inputs these are: nominal active power of the inverter P_n , nominal grid frequency ω_n ,

and carrier PWM switching frequency f_{sw} . This is followed by the introduction of the impedance base value Z_b characterized by:

$$Z_b = \frac{E_n^2}{P_n}, \quad (1)$$

and the capacitance base value C_b , respectively, denoted as:

$$C_b = \frac{1}{\omega_n Z_b}, \quad (2)$$

where E_n is the line-to-line Root-Mean-Square (RMS) voltage. These base values are used to scale the LCL filter values as percentages of the base values for subsequent design procedure steps. For completeness, it is worth noting that the base value of the inductance may be calculated as:

$$L_b = \frac{Z_b}{\omega_n}, \quad (3)$$

where Z_b is from Equation (1) and ω_n as previously [13]. The proposed design procedure by Liserre *et al.* [6] introduces design principles on the filter capacitance C_f , inductance L_f , resonance frequency f_{res} , and the damping characteristics. More specifically, these are subject to the following constraints in:

1. The amount of filter capacitance C_f is limited by the drop in power factor being less than a predetermined margin at the rated power.
2. The total amount of filter inductance L_f being less than a predetermined value.
3. The filter resonance frequency f_{res} being greater than ten times the grid frequency f_g and less than one-half of the carrier's PWM switching frequency f_{sw} .
4. The passive damping being such that oscillation is avoided, but without significantly reducing the efficiency.

The performance and effectiveness of the solution is evaluated by five performance characteristics, where three of them are concerning low-frequency (≤ 2.5 kHz) and two high-frequency (2.5–20 kHz) performance of the solution. These characteristics are as follows:

1. Total Harmonic Distortion (THD) of the current.
2. Power Factor (PF).
3. Average of the absolute error of DC voltage Δu_0 .

4. The largest sideband of the switching frequency current harmonic $I_{\langle h_{sw} \rangle}$ content near f_{sw} .
5. The near switching frequency RMS current value $I_{\text{rms,sw}}$ of the high-frequency harmonic content as a percentage of the fundamental current harmonic $I_{\langle 1 \rangle}$.

The THD can be expressed as a ratio of the square root on the sum of squared harmonics $h = 2, 3, \dots, H$ with respect to the first fundamental harmonic of the given complex input signal I , which can be written as:

$$\text{THD}_I = \frac{\sqrt{\sum_{h=2}^H I_{\langle h \rangle}^2}}{I_{\langle 1 \rangle}} 100\%, \quad (4)$$

where $I_{\langle h \rangle}$ is the h^{th} current harmonic and H is the upper bound of harmonics to include in. Here, Liserre *et al.* [6] have opted for use harmonics up to $H = 50$. Respectively, the PF can also be expressed through a given inputs signal I denoted by:

$$\text{PF}_I = \frac{I_{\langle 1 \rangle}}{I} \cos \varphi, \quad (5)$$

where I is now the overall RMS value of the current and φ is the angle between the fundamental current and voltage. Finally, the RMS value of the high-frequency harmonic content $I_{\text{rms,sw}}$ is:

$$I_{\text{rms,sw}} = \sqrt{\sum_{h=H+1}^K I_{\langle h \rangle}^2}, \quad (6)$$

where the harmonics $h = H + 1, H + 2, \dots, K$ are included, K being the upper bound on the harmonics. Recalling from the above, $H = 50$ being defined as the upper bound harmonic for the THD of the current, but in terms of Equation (6) the lower bound will be $H = 51$ and respectively the upper bound $K = 400$. The VSI-side inductance L_i and grid-side inductance L_g is governed by the relation:

$$L_g = rL_i, \quad (7)$$

where r is a proportionality constant between the grid-side L_g and inverter-side L_i inductance values. The LCL filter capacitance C_f shall be expressed as the product:

$$C_f = xC_b, \quad (8)$$

where x is the percentage of reactive power absorbed in rated conditions and C_b as previously in Equation (2). Respectively, the current ripple attenuation near the h^{th} harmonic of the switching frequency h_{sw} , neglecting the losses and damping of the LCL filter, is

expressed by the ratio of the h^{th} harmonic of the grid-side current $i_{g,\langle h_{\text{sw}} \rangle}$ with respect to $i_{i,\langle h_{\text{sw}} \rangle}$ and denoted by:

$$\frac{i_{g,\langle h_{\text{sw}} \rangle}}{i_{i,\langle h_{\text{sw}} \rangle}} = \frac{1}{|(1 + r(1 - ax))|}, \quad (9)$$

where r and x as in Equations (7) and (8) earlier. Then the h^{th} switching harmonic of the VSI-side current i_i and grid-side current i_g as in the equivalent per-phase model of a three-phase LCL filter depicted in Figure 3. The constant a in Equation (10), is defined as:

$$a = L_i C_b f_{\text{sw}}^2, \quad (10)$$

where L_i and C_b as in Equations (7) and (8), respectively, with f_{sw} being a design constant. The resonance frequency f_{res} is governed by:

$$f_{\text{res}} = \sqrt{\frac{L_f}{L_i L_g C_f}}, \quad (11)$$

where L_f is the total amount of inductance, that is $L_f = L_i + L_g$, in the LCL filter [6]. Finally, the step-by-step LCL filter design procedure can be formalized as Algorithm 1.

Algorithm 1 LCL filter design procedure by Liserre *et al.* [6].

1. Set the inverter side inductance L_i proportional to the grid-side inductance L_g by factor r , as in Equation (7), such that desired level of current ripple on the VSI-side is achieved.
 2. Select the absorbed amount of reactive power at rated power by determining the C_f capacitance value such that Equation (8) is satisfied, while taking into account Constraint 1. on the C_f value.
 3. Determine the targeted level of current ripple reduction on the grid-side by selecting the amount of L_g such that the Constraint 2. and Equation (9) are satisfied.
 4. Evaluate the resulting resonance frequency f_{res} with Equation (11), while bearing in mind Constraint 3. by repeating Steps 2. or 3. until the condition for f_{res} is satisfied.
 5. Choose the desired level of damping in accordance to Constraint 4. and evaluate whether the LCL attenuation is sufficient or not; repeat Steps 2. and 3. if necessary.
 6. Finally, validate the LCL filter attenuation in alternative switching frequency and load conditions.
-

It is worth noting, that the wye-configuration of the filter capacitance C_f streamlines the three-phase LCL filter modelling and design, such that a per-phase equivalent model can

be utilized [1, 6]. An equivalent per-phase circuit diagram of a three-phase LCL filter is depicted in Figure 3 with VSI-side u_i and grid-side u_g voltages as variables that have not been introduced earlier. An alternative LCL filter design procedure with an iterative

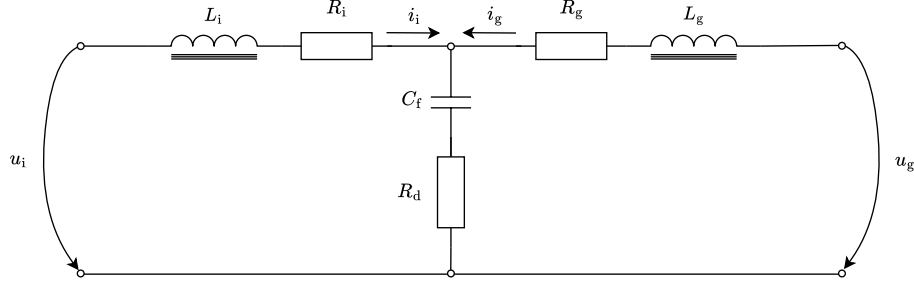


Figure 3. LCL filter per-phase model adapted from Reznik *et al.* [1] and Liserre *et al.* [6].

step-by-step approach is proposed by Reznik *et al.* [1]. It bears many similarities to the one proposed by Liserre *et al.* [6], but deviating by the chosen mathematical modelling approach and the damping solution. Additionally the paper by Reznik *et al.* [1] considers, both, wye- and delta-connected capacitor configurations, where as Liserre *et al.* [6] the wye-connected configuration is only explored. The significant distinction between the two proposed design procedures is the of principle on how the LCL filter damping is implemented. In the paper by Liserre *et al.* [6], both active and passive damping, and jointly employed with a VSI and LCL filter, while Reznik *et al.* [1] are employing only passive damping. Consequently, Reznik *et al.* [1] are providing quantifiable design constraint for the LCL filter damping resistor R_d sizing denoted by the following:

$$R_d = \frac{1}{3f_{\text{res}}C_f}, \quad (12)$$

where f_{res} is as in Equation (11) earlier. While the practical LCL filter design procedure by Reznik *et al.* [1] bears many similarities with Liserre *et al.* [6], it does additional quantifiable guidance such as for the damping resistance value R_d . The procedure starts by deriving the Z_b and C_b values from the input parameters P_n , f_g , f_{sw} , u_g , and DC voltage u_{dc} . Next, the procedure is continued with the selection of C_f and L_i values. Then to be followed by the identification of the attenuation factor k_a and the respective grid-side inductance L_g values. The attenuation factor k_a is essentially attained by applying Equation (10) to (9) and rewriting it as

$$k_a = \frac{i_{g,\langle h_{\text{sw}} \rangle}}{i_{i,\langle h_{\text{sw}} \rangle}} = \frac{1}{|(1 + r(1 - L_i C_b f_{\text{sw}}^2 x))|}. \quad (13)$$

Upon the identification of the k_a value, similarly to Liserre *et al.* [6], the condition for $10f_g < f_{res} < 0.5f_{sw}$ should be satisfied or otherwise new values for k_a and L_g should be selected. Once the f_{res} constraint has been satisfied, the value of the damping resistance R_d can be determined. Finally, depending on the chosen capacitor configuration, detailed characteristics of the inductances can be defined. The flowchart diagram of the full step-by-step design procedure by Reznik *et al.* [1] is depicted in Figure 4.

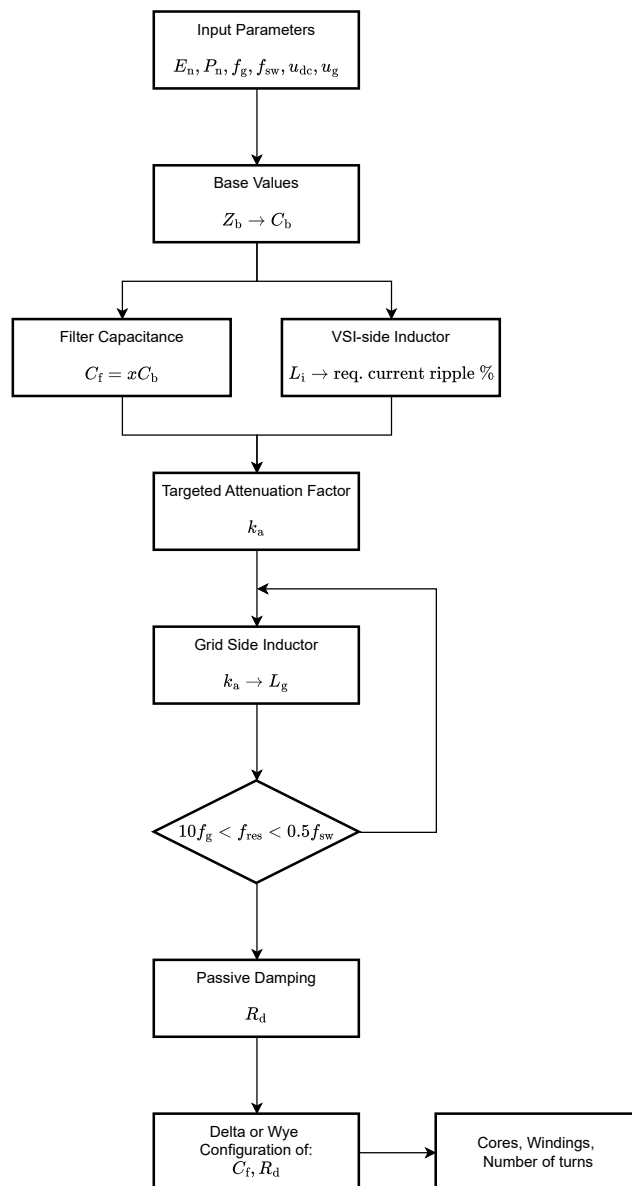


Figure 4. Flowchart diagram of a LCL filter design procedure inspired by Reznik *et al.* [1].

2.2 Optimisation

One alternative for an optimisation-based approach is to represent the system as a parametric model such that the residual of the model, at its estimated parameter values, with respect to the desired design objectives is minimized [14]. Examples of such optimisation frameworks are the Least Squares (LSQ) and Nonlinear Least Squares (NLSQ) methods with the general setting described by:

$$F_{\text{obj}}(\mathbf{x}) := \underset{\mathbf{x}}{\operatorname{argmin}} \sum_{i=1}^N (\mathbf{y}_i - f(\mathbf{x}_i))^2, \quad (14)$$

where F_{obj} is the objective function to be minimized (or maximized), \mathbf{x} a vector of input parameters, \mathbf{y} a vector of reference values, N the number of parameters, \mathbf{y}_i is the i^{th} reference, and finally \mathbf{x}_i is the i^{th} input parameter value of $f(\cdot)$ [15]. The mathematical model $f(\cdot)$ is linear in LSQ and non-linear in NLSQ cases [15].

Consequently, the research community has proposed NLSQ based system parameter optimisation design procedures, for both L and LCL filter topologies, such as in [4, 14, 16, 17]. Moreover, Gurrola-Corral *et al.* [4] propose a LCL filter parameter identification procedure that is founded on two core principles: NLSQ as the optimisation method and Extended Harmonic Domain (EHD) as the system modelling method [4, 16–18]. With these the LCL filter parameter identification procedure steps can be characterized as described in Algorithm 2.

Algorithm 2 LCL filter design procedure by Gurrola-Corral *et al.* [4].

1. Formulation of the equivalent EHD model.
 2. Computation of the EHD steady-state solution \mathbf{X}_{ss} .
 3. Evaluation of the estimated system performance characteristics \mathbf{p}_{est} .
 4. Evaluation of the objective function $F(\mathbf{x}^{(k)})$ with respect to the system reference performance characteristics \mathbf{p}_{ref} .
 5. Finally, has the minimum been found?
-

A favourable property of the EHD method is its capability of capturing the harmonic content of the electric signals up to the h^{th} harmonic, such that the Linear Time Periodic (LTP) system can be represented as time-domain Linear Time Invariant (LTI) system [4, 16–18].

long as the control variables of the modulation method are known, is described by:

$$\mathbf{D} = \text{diag}(-jh\omega_0, \dots, -j\omega_0, 0, j\omega_0, \dots, jh\omega_0), \quad (19)$$

where the diagonal elements are derived from the product of vector basis functions $\mathbf{G}(t)$ and \mathbf{D} , such that $\dot{\mathbf{G}}(t) = \mathbf{G}(t)\mathbf{D}$ holds. The contents of the vector $\mathbf{G}(t)$ is defined as

$$\mathbf{G}(t) = [e^{-jh\omega_0 t}, \dots, e^{-j\omega_0 t}, \dots, 1, \dots, e^{j\omega_0 t}, \dots, e^{jh\omega_0 t}]. \quad (20)$$

Then, the state-vector $\mathbf{X}(t)$ is written as:

$$\mathbf{X}(t) = [\mathbf{X}_{(-h)}(t), \dots, \mathbf{X}_{(-1)}(t), \mathbf{X}_{(0)}(t), \mathbf{X}_{(1)}(t), \dots, \mathbf{X}_{(h)}(t)]^T, \quad (21)$$

where the element $\mathbf{X}_{(k)}(t)$ is the k^{th} harmonic content of the time-period signal $x(t)$. Finally, the EHD steady-state solution of the system is achieved by setting $\dot{\mathbf{X}}(t) = 0$ from Equation (17) and solving for \mathbf{X}_{ss} as shown by:

$$\mathbf{X}_{\text{ss}} = -(\mathbf{A} - \mathbf{D})^{-1}\mathbf{B}\mathbf{U}, \quad (22)$$

where the steady-state solution \mathbf{X}_{ss} is $\mathbf{X}(t)$ from Equations (17) and (21) [16, 18].

Upon the introduction of EHD model derivation, each step of the LCL filter parameter identification algorithm by Gurrola-Corral *et al.* [4] can now be explored in further detail. Namely, the first step is to construct a EHD equivalent model of the system, Equation (17), and form the initial state-vector $\mathbf{x}^{(0)}$, which is populated by a initial guess of the desired design parameters [4]. Gurrola-Corral *et al.* [4] have chosen here: filter elements (L_g, C_f, L_i, R_d), DC-link capacitance C_{dc} , modulation amplitude m_a , and modulation phase-shift θ_m denoted as:

$$\mathbf{x}^{(0)} = [L_g, C_f, L_i, R_d, C_{\text{dc}}, m_a, \theta_m], \quad (23)$$

where the last two elements (m_a, θ_m) are the SPWM modulation parameters. In the second step of the algorithm the EHD steady-state solution is being computed with

$$\mathbf{X}_{\text{ss}} = -(\mathbf{A}(\mathbf{x}^{(k)}) - \mathbf{D})^{-1}\mathbf{B}(\mathbf{x}^{(k)})\mathbf{U}, \quad (24)$$

where the matrices \mathbf{A} and \mathbf{B} are from Equation (22) have been augmented to take in the k^{th} iteration of the state-vector $\mathbf{x}^{(k)}$, which is the initial-state vector $\mathbf{x}^{(0)}$ when $k = 0$ [4]. The third step is to evaluate the estimated system performance characteristics \mathbf{p}_{est} with respect to the steady-state solution \mathbf{X}_{ss} [4]. The \mathbf{p}_{est} is a collection of system performance characteristics that can be for example: PF, f_{res} , THD, Total Demand Distortion (TDD), active

power P , or reactive power Q . A desired subset of application dependent characteristics are selected into the \mathbf{p}_{est} vector as exemplified by

$$\mathbf{p}_{\text{est}} = [\text{PF}, \text{THD}_u, \text{THD}_i, P, f_{\text{res}}, \dots]. \quad (25)$$

The fourth step is the evaluation of the objective function $F(\mathbf{x}^{(k)})$ with respect to the system reference performance characteristics \mathbf{p}_{ref} [4]. This should correspond with the elements of \mathbf{p}_{est} that were the previously chosen performance characteristics, but this time rather as respective reference characteristics denoted by the (*) superscripts in

$$\mathbf{p}_{\text{ref}} = [\text{PF}^*, \text{THD}_u^*, \text{THD}_i^*, P^*, f_{\text{res}}^*, \dots]. \quad (26)$$

Finally, in the fifth and final step, at each k^{th} iteration of the optimisation loop, the objective function from Equation (27) is evaluated with the state-vector $\mathbf{x}^{(k)}$ for comparing whether a minimum of the objective function has been located or not:

$$F(\mathbf{x}^{(k)}) := \underset{\mathbf{x}^{(k)}}{\text{argmin}} \sum_{n=1}^N \rho_n^2 (\mathbf{p}_{\text{ref},n} - \mathbf{p}_{\text{est},n}(\mathbf{x}^{(k)}))^2, \quad (27)$$

where N is the number of performance characteristics, n is the n^{th} element of the $(\boldsymbol{\rho}, \mathbf{p}_{\text{ref}}, \mathbf{p}_{\text{est}})$ vectors, and $\boldsymbol{\rho}$ is a vector of weights denoting the relative importance of the characteristic [4]. If the minimum was located then the identified design parameters can be read from the state-vector $\mathbf{x}^{(k)}$, otherwise the vector contents are updated for the next iteration of the algorithm [4]. The state-vector $\mathbf{x}^{(k)}$ can be subjected to some constraints in accordance with

$$\text{subject to: } \mathbf{x}^{\text{L}} \leq \mathbf{x}^{(k)} \leq \mathbf{x}^{\text{U}}, \quad (28)$$

where the vectors \mathbf{x}^{L} and \mathbf{x}^{U} are lower and upper bounds of the $\mathbf{x}^{(k)}$ respectively [16]. Finally, the algorithm by Gurrola-Corral *et al.* [4] can be summarized by the flowchart depicted in Figure 5.

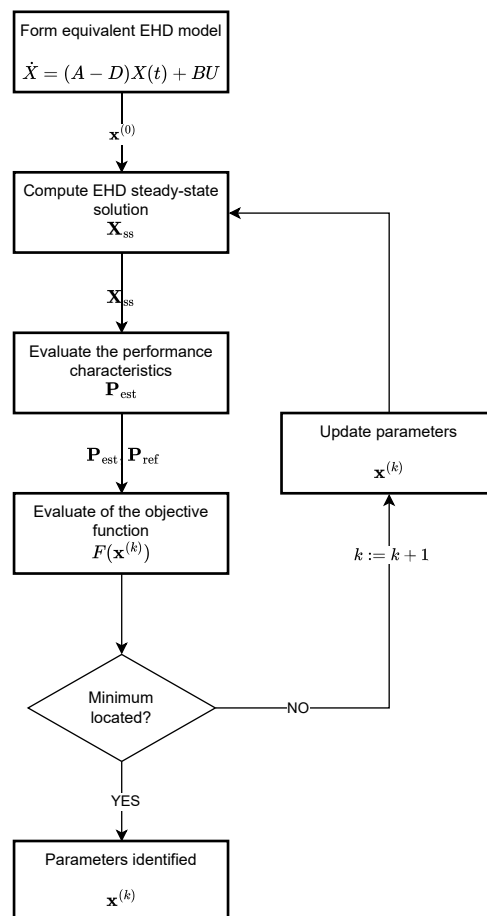


Figure 5. NLSQ and EHD model parameter identification algorithm flowchart adapted from Gurrola-Corral *et al.* [4].

3 PROPOSED METHODS

This section describes the equations, algorithms, and methods used to address the main research question presented in Section 1. There are dedicated subsections exploring the details of each respective topic. The proposed methods are addressing the LCL filter design parameter identification problem and its first four objectives by describing:

1. The mathematical VSI-model simulating the behaviour of a simple VSI device (Objective 1).
2. The mathematical LCL-model simulating the behaviour of the filter (Objective 2).
3. The selected performance metrics, which in this setting are electrical quality characteristics (Objective 3).
4. The principle of the DE global optimisation method for searching the design parameters of the LCL filter (Objective 4).

While these are covered by the Sections 3.1, 3.2, 3.3, and 3.4; the remaining two objectives: construction of simulation environment (Objective 5) and evaluation of the feasibility of the obtained solution, by virtue of DE global optimisation search (Objective 6), will be addressed in Section 4.

3.1 VSI-model

In order to transfer electrical energy between AC and DC systems, respective energy conversion must be conducted, such that the energy can flow between the systems [1, 4]. While, the LCL filter has an important role in adapting the two systems it is, nevertheless, important to introduce the concept of VSI modulation techniques. There exist alternative modulation strategies in implementing a functioning three-phase two-level VSI device, such as: Sawtooth-SPWM, Triangle-SPWM, or Space Vector Modulation (SVM) to name a few [19, 20].

The objective of the SPWM modulation is to control the switching of the VSI's semiconductor switches to *OPEN* and *CLOSED* states by generating desired switching patterns to the respective phases to drive some load from a fixed DC voltage source [21]. This type of a VSI topology is depicted in Figure 6, where the VSI's semiconductor switches

are denoted as T_1-T_6 , controlled by a discontinuous SPWM switching functions, with the respective bridge diodes D_1-D_6 . Each phase has top and bottom pairs of switches and diodes for producing SPWM switched output, where in Figure 6 (D_1, T_1) are the top and (D_4, T_4) the bottom pairs for the first phase a . Similarly for the second phase b , they are (D_3, T_3) for the top and (D_6, T_6) for the bottom. Finally, (D_5, T_5) and (D_2, T_2) are the top and bottom pairs of the last phase c . The discontinuous SPWM switching functions of

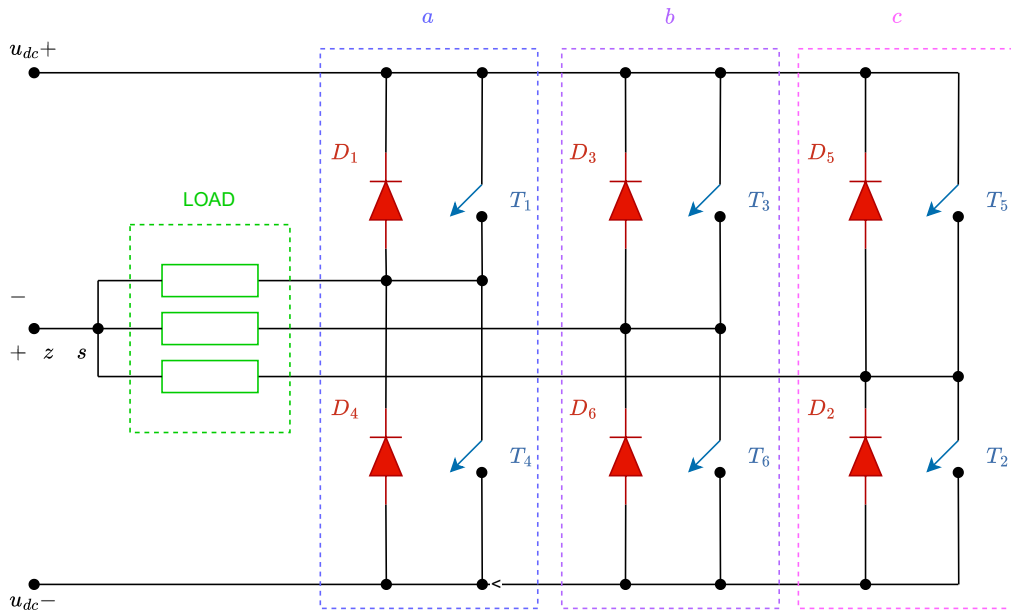


Figure 6. Three-phase two-level VSI inspired by Holmes and Lipo [21].

a three-phase VSI can be derived from a system of equations, resulting into a discrete switching function for each phase [21]. Denoting the values of the switches T_1-T_6 with m_1-m_6 , where m_x , $x \in \{1, 2, \dots, 6\}$ takes the value '0' when the switch is *OPEN* and '1' when it is *CLOSED*. The SPWM switched voltage function can be expressed as:

$$\begin{cases} u_{az} = u_{dc}(m_1 - m_4), \\ u_{bz} = u_{dc}(m_3 - m_6), \\ u_{cz} = u_{dc}(m_5 - m_2), \end{cases} \quad (29)$$

where u_{dc} is the fixed DC-link voltage of the VSI [21]. Since the top and bottom switches of each phase cannot be in *CLOSED* state at the same time, additional constraint should

be imposed. Collecting these constraints into a system of equations denoted by:

$$\begin{cases} m_1 + m_4 = 1, \\ m_3 + m_6 = 1, \\ m_5 + m_2 = 1, \end{cases} \quad (30)$$

such that applying them to Equation (29), the final form can be obtained [21]. This can be expressed as a time dependent equation on t :

$$\begin{cases} u_{az}(t) = u_{dc}(2s_a(t) - 1), \\ u_{bz}(t) = u_{dc}(2s_b(t) - 1), \\ u_{cz}(t) = u_{dc}(2s_c(t) - 1), \end{cases} \quad (31)$$

where $s_a(t) = m_1(t)$, $s_b(t) = m_3(t)$, and $s_c(t) = m_5(t)$ are the sought out discontinuous SPWM switching functions. From here onward it is worth noting that, while the practical real-world applications may often be implemented with a three-phased VSI, for the purpose of describing the methods proposed it in this work suffices to focus on a single-phase implementation. This is driven by the fact that the phases of a three-phased VSI may be assumed to be symmetrical, but with a 120° phase-shifted switching pattern with respect to each other, under reasonable circumstances. For a detailed treatment on three-phased PWM modulation techniques, in general, the reader is referred to book by Holmes and Lipo [22].

Recalling the two alternatives for generating SPWM modulation carrier waveforms, namely, Sawtooth-SPWM and Triangle-SPWM from earlier – it is reasonable to introduce them now. Both generator functions can, for example, be derived through Fourier series representations [19] or alternatively by utilising some accompanying toolbox or library in desired programming environment. However, the author of this work did opt to implement both of these functions as algorithms in the selected programming environment, namely MATLAB, albeit both functions would have been available from the *Signal Processing Toolbox* of the chosen programming environment.

The name of the Sawtooth function refers to the shape of the output that the function produces once evaluated at given points x . The author's implementation of the Sawtooth carrier waveform generator function is described in Algorithm 3.

Algorithm 3 Sawtooth-SPWM waveform generator function (sawtooth).

Input:

$\mathbf{x}_{1:N}$ = Vector of function evaluation points.

Output:

$\mathbf{y}_{1:N}$ = Vector of function values evaluated at points $\mathbf{x}_{1:N}$.

1. Set carrier period:

$$T_c \leftarrow 2\pi.$$

2. Compute the modulus $\mathbf{T}_{x,1:N}$ with respect to $\mathbf{x}_{1:N}$ and period T_c :

$$\mathbf{T}_{x,1:N} \leftarrow (\mathbf{x}_{1:N} \bmod T_c).$$

3. Compute the ratios $\mathbf{x}_{\text{rising}}$ with respect to $\mathbf{T}_{x,1:N}$ and period T_c :

$$\mathbf{x}_{\text{rising},1:N} \leftarrow (\mathbf{T}_{x,1:N}/T_c).$$

4. Interpolate the rising edge output values at $\mathbf{x}_{\text{rising},1:N}$ from the interval $[-1.0, 1.0)$:

$$\mathbf{y}_{1:N} \leftarrow \text{lerp}(-1.0, \mathbf{x}_{\text{rising},1:N}, 1.0).$$

Similarly, the Triangle function is modified version of the Algorithm 3 as defined by Algorithm 4. The jointly used lerp function in Algorithms 3 and 4 is a linear interpolation

Algorithm 4 Triangle-SPWM waveform generator function (triangle).

Input:

$\mathbf{x}_{1:N}$ = Vector of function evaluation points.

Output:

$\mathbf{y}_{1:N}$ = Vector of function values evaluated at $\mathbf{x}_{1:N}$.

1. Set carrier period and compute its mid-point:

$$T_c \leftarrow 2\pi, T_{\frac{c}{2}} \leftarrow T_c/2.$$

2. Compute the modulus $\mathbf{T}_{x,1:N}$ with respect to $\mathbf{x}_{1:N}$ and period T_c :

$$\mathbf{T}_{x,1:N} \leftarrow (\mathbf{x}_{1:N} \bmod T_c).$$

3. Compute whether the points $\mathbf{x}_{1:N}$ lies on the rising or falling half period of T_c :

$$\mathbf{E}_{\text{rising},1:N} \leftarrow (\mathbf{T}_x \leq T_{\frac{c}{2}}), \mathbf{E}_{\text{falling},1:N} \leftarrow (\mathbf{T}_x > T_{\frac{c}{2}}).$$

4. Compute the ratios $\mathbf{x}_{\text{rising},1:N}$ and $\mathbf{x}_{\text{falling},1:N}$ with respect to $\mathbf{T}_{x,1:N}$ and $T_{\frac{c}{2}}$:

$$\mathbf{x}_{\text{rising},1:N} \leftarrow (\mathbf{T}_{x,1:N}/T_{\frac{c}{2}}), \mathbf{x}_{\text{falling},1:N} \leftarrow ((\mathbf{T}_{x,1:N} - T_{\frac{c}{2}})/T_{\frac{c}{2}}).$$

5. If $\mathbf{E}_{\text{rising},1:N}$ then interpolate the output value at $\mathbf{x}_{\text{rising},1:N}$ from the interval $[-1.0, 1.0)$:

$$\mathbf{y}_{1:N} \leftarrow \text{lerp}(-1.0, \mathbf{x}_{\text{rising},1:N}, 1.0).$$

6. If $\mathbf{E}_{\text{falling}}$ then interpolate the output value at $\mathbf{x}_{\text{falling},1:N}$ from the interval $(1.0, -1.0]$:

$$\mathbf{y}_{1:N} \leftarrow \text{lerp}(1.0, \mathbf{x}_{\text{falling},1:N}, -1.0).$$

function denoted by:

$$\text{lerp}(l, \mathbf{x}, u) = (u - l) \min(1.0, \max(\mathbf{x}, 0.0)) + l, \quad (32)$$

which outputs a value from a semi-closed interval $[l, u)$, governed by the factor x , where: $l \in [-1.0, 1.0)$, $u \in [-1.0, 1.0)$, $l < u$, and $\mathbf{x} \in [0.0, 1.0)$. By the virtue of previous results on introducing the Sawtooth and the Triangle carrier generator functions, the final SPWM discontinuous switching function may be devised. Essentially, the objective of the discontinuous SPWM switching function is to compare the generated Sawtooth or Triangle carrier waveform to the fundamental waveform in either Sawtooth-SPWM or Triangle-SPWM modulation schemes [19]. Combining the fundamental waveform generation with either of the carrier waveform generator functions, completes the SPWM modulation method for controlling the switches T_1 - T_6 in Figure 6.

There are, though, two equations that should be introduced first for the purpose of generating the fundamental wave, which corresponds to the AC grid waveform. The first formula is for calculating the angular frequency of the wave, denoted by:

$$\omega_0 = 2\pi f = \frac{2\pi}{T_0}, \quad (33)$$

where ω_0 is the angular frequency in rad/s, f frequency in Hz, and T_0 period in s of the wave. The latter equation is for constructing the actual fundamental wave described by:

$$F_0(t) = m_a \sin(\omega_0 t + \theta_0), \quad (34)$$

where $F_0(t)$ is the value of the wave at time instance t in s, m_a modulation amplitude ($m_a \geq 0$), ω_0 angular frequency, and phase-shift θ_0 in rad. Finally, merging the previous results from Algorithms 3 and 4 with Equations (32), (33), and (34) into Algorithm 5, a method for computing the individual discontinuous switching functions for each phase of a three-phase two-level VSI is obtained.

Algorithm 5 SPWM modulation per-phase discontinuous switching function (spwm).

Input:

$\mathbf{t}_{1:T}$ = Time instance of the discontinuous switching function evaluation.

m_a = Modulation amplitude.

T_0 = Fundamental wave period.

T_c = Carrier wave period.

θ_0 = Fundamental wave phase-shift.

θ_c = Carrier wave phase-shift.

C_x = Carrier wave generation method.

Output:

$\mathbf{S}_{1:T}$ = Value of discontinuous switching function at times $\mathbf{t}_{1:T}$.

$\mathbf{F}_{0,1:T}$ = Value of the fundamental wave at times $\mathbf{t}_{1:T}$.

$\mathbf{F}_{c,1:T}$ = Value of the carrier wave at times $\mathbf{t}_{1:T}$

1. Compute angular frequency of the fundamental wave:
 $\omega_0 \leftarrow 2\pi/T_0$.
 2. Compute the value of the fundamental wave:
 $\mathbf{F}_{0,1:T} \leftarrow m_a \sin(\omega_0 \mathbf{t}_{1:T} + \theta_0)$.
 3. Compute angular frequency of the carrier wave:
 $\omega_c \leftarrow 2\pi/T_c$.
 4. If C_x is Sawtooth then compute the value of the carrier wave:
 $\mathbf{F}_{c,1:T} \leftarrow \text{sawtooth}(\omega_c \mathbf{t}_{1:T} + \theta_c)$.
 5. Else C_x is Triangle and compute the value of the carrier wave :
 $\mathbf{F}_{c,1:T} \leftarrow \text{triangle}(\omega_c \mathbf{t}_{1:T} + \theta_c)$.
 6. Compute the value of the discontinuous switching function and return:
 $\mathbf{S}_{1:T} \leftarrow (\mathbf{F}_{0,1:T} < \mathbf{F}_{c,1:T})$
-

3.2 LCL-model

In order to model the behaviour of the LCL in the system with an AC grid and VSI, such as in Figure 2, a mathematical model of the LCL needs to be established. In the interest of the scope of this work, the detailed derivation of a Node-Voltage and Mesh-Current circuit analysis modelling process will be omitted, but rather, an existing model shall be used instead. There are a number of alternative models of LCL circuit with subtle differences, such as whether additional grid-side inductances are incorporated or not, that could be applied here [1, 4, 6, 16]. For the purpose of this work the state-space model by Reznik *et al.* [1] shall be used. In the aforementioned paper the LCL circuit was described

as a first-order Ordinary Differential Equation (ODE) system of equations as denoted as:

$$\begin{cases} \frac{d}{dt}i_i(t) &= \frac{1}{L_i}(u_i(t) - u_{C_f}(t) - R_d(i_i(t) - i_g(t)) - R_i i_i(t)), \\ \frac{d}{dt}i_g(t) &= \frac{1}{L_g(u_{C_f}(t) + R_d(i_i(t) - i_g(t)) - u_g(t) - R_g i_g(t))}, \\ \frac{d}{dt}u_{C_f}(t) &= \frac{i_i(t) - i_g(t)}{C_f}, \end{cases} \quad (35)$$

where $\frac{d}{dt}i_i(t)$, $\frac{d}{dt}i_g(t)$, and $\frac{d}{dt}u_{C_f}(t)$ are the differentials with respect to time of i_i , i_g , and voltage u_{C_f} over capacitor C_f that has not been previously introduced. Since, Equation (35) is a system of equations solved with respect to the time differentials – some integration method needs to be applied to compute the respective instantaneous values. Considering that a computer program will be used to solve the problem, a numerical integration method is required. Coincidentally, there are plethora of ODE numerical integration methods developed over time, such as: Euler, leapfrog, modified Euler, Runge-Kutta (RK), and Rosenbrock to mention a few [23]. These numerical ODE integration approaches are based on either Fixed- and Variable-step evaluation of the solution [24]. Numerical programming environments, such as MATLAB, typically offer many alternative ODE solvers depending on the whether the system under modelling is stiff or non-stiff by nature [25,26].

The approach adopted in this work is based on the principle that the LCL system behaviour is modelled accurately at each time step Δt of the simulation. This lead to the conclusion that the numerical ODE solver should be Fixed-step rather than Variable-step based. Consequently, an own adaptation of the RK method was employed rather than commercially readily available, which is based on the fourth-order version of it, such that:

$$y_{n+1} = y_n + \frac{h}{6}(z_1 + 2z_2 + 2z_3 + z_4), \quad (36)$$

where z_1 , z_2 , z_3 , and z_4 are defined as:

$$\begin{aligned} z_1 &= f(t_n, y_n), \\ z_2 &= f\left(t_n + \frac{h}{2}, y_n + h\frac{z_1}{2}\right), \\ z_3 &= f\left(t_n + \frac{h}{2}, y_n + h\frac{z_2}{2}\right), \\ z_4 &= f(t_n + h, y_n + h z_3), \end{aligned} \quad (37)$$

with $h, h > 0$ being the time step, y_n solution evaluated at n^{th} iteration t_n , and finally y_{n+1} evaluated at the $(n + 1)^{\text{th}}$ iteration [27]. Plugging the results from Equations (36) and (37) into Equation (35), a procedure for numerically solving the LCL ODE model is obtained, described in Algorithm 6.

Algorithm 6 Fourth-order Runge-Kutta numerical solver for the LCL ODE (lcloderk4).

Input:

$\mathbf{t}_{1:T}$ = Time at indices: $1, 2, \dots, T$.

$\mathbf{i}_{1:2}^{(0)}$ = Initial conditions for VSI- and grid-side phase currents: $i_i(0), i_g(0)$.

$\mathbf{u}_{1:2}$ = Time dependent voltage functions: u_i, u_g .

$\mathbf{p}_{1:6}$ = Model parameters: $L_i, R_i, C_f, R_d, L_g, R_g$.

Output:

$\mathbf{i}_{i,1:T}$ = VSI-side phase current at times $\mathbf{t}_{1:T}$.

$\mathbf{i}_{g,1:T}$ = Grid-side phase current at times $\mathbf{t}_{1:T}$.

$\mathbf{u}_{C_f,1:T}$ = Capacitor C_f voltage at times $\mathbf{t}_{1:T}$.

1. Decompose initial conditions and voltage functions:

$$i_i(0) \leftarrow \mathbf{i}_1^{(0)}, i_g(0) \leftarrow \mathbf{i}_2^{(0)}, u_i \leftarrow \mathbf{u}_1, \text{ and } u_g \leftarrow \mathbf{u}_2.$$

2. Decompose model parameters:

$$L_i \leftarrow \mathbf{p}_1, R_i \leftarrow \mathbf{p}_2, C_f \leftarrow \mathbf{p}_3, R_d \leftarrow \mathbf{p}_4, L_g \leftarrow \mathbf{p}_5, R_g \leftarrow \mathbf{p}_6.$$

3. Populate matrix \mathbf{A} with model parameters L_i, R_i, C_f, R_d, L_g , and R_g :

$$\mathbf{A} \leftarrow \begin{bmatrix} -((R_i + R_d)/L_i) & R_d/L_i & -(1/L_i) \\ R_d/L_g & -((R_g + R_d)/L_g) & (1/L_g) \\ (1/C_f) & -(1/C_f) & 0 \end{bmatrix}.$$

4. Populate matrix \mathbf{B} with model parameters L_i and L_g :

$$\mathbf{B} \leftarrow \begin{bmatrix} (1/L_i) & 0 \\ 0 & (1/L_g) \\ 0 & 0 \end{bmatrix}.$$

5. Initialize vector \mathbf{x} with initial conditions $i_i(0)$ and $i_g(0)$:

$$\mathbf{x}_{:,1} \leftarrow \begin{bmatrix} i_i(0) \\ i_g(0) \\ (i_i(0) - i_g(0))/C_f \end{bmatrix}.$$

6. Populate vector $\mathbf{u}(t)$ with model measurement inputs $u_i(t)$ and $u_g(t)$:

$$\mathbf{u}(t) \leftarrow \begin{bmatrix} u_i(t) \\ u_g(t) \end{bmatrix}.$$

7. Define state-space matrix function:

$$f(\mathbf{x}, \mathbf{u}) \leftarrow \mathbf{A}\mathbf{x} + \mathbf{B}\mathbf{u}.$$

8. For each time step $n = 2, 3, \dots, T$ using RK solve the LCL state-space model:

$$\begin{aligned} z_1 &\leftarrow f(\mathbf{x}_{:,n-1}, \mathbf{u}(\mathbf{t}_{n-1})), \\ z_2 &\leftarrow f(\mathbf{x}_{:,n-1} + h\frac{z_1}{2}, \mathbf{u}(\mathbf{t}_{n-1}) + \frac{h}{2}), \\ z_3 &\leftarrow f(\mathbf{x}_{:,n-1} + h\frac{z_2}{2}, \mathbf{u}(\mathbf{t}_{n-1}) + \frac{h}{2}), \\ z_4 &\leftarrow f(\mathbf{x}_{:,n-1} + h z_3, \mathbf{u}(\mathbf{t}_{n-1}) + h), \\ \mathbf{x}_{:,n} &\leftarrow \mathbf{x}_{:,n-1} + \frac{h}{6}(z_1 + 2z_2 + 2z_3 + z_4). \end{aligned}$$

9. Return VSI-side current \mathbf{i}_i , grid-side current \mathbf{i}_g , and capacitor voltage \mathbf{u}_{C_f} :

$$\mathbf{i}_{i,1:T} \leftarrow \mathbf{x}_{i,1:T}, \mathbf{i}_{g,1:T} \leftarrow \mathbf{x}_{2,1:T}, \mathbf{u}_{C_f,1:T} \leftarrow \mathbf{x}_{3,1:T}.$$

3.3 Performance characteristics

From the previously introduced the VSI- and LCL-models the desired system performance characteristics may be derived. These characteristics may be used to assess the the fitness of the solution with respect to the LCL model parameter state-vector $\mathbf{x}^{(k)}$ at k^{th} evaluation step of the optimisation procedure. Recalling the reference system diagram depicted in Figure 2 it is evident that the selected characteristics should capture the key characteristics of the system, such that the corresponding optimisation goals may be achieved. Adopting the convention from Section 2.2, the estimated performance characteristics at k^{th} iteration of the optimisation procedure shall be denoted as \mathbf{p}_{est} and the respective goals as the reference performance characteristics \mathbf{p}_{ref} . The chosen elements of the characteristics \mathbf{p}_{est} and \mathbf{p}_{ref} are listed in Table 1 with their respective descriptions.

Table 1. Estimated and reference performance characteristics.

Element	\mathbf{p}_{est}	\mathbf{p}_{ref}	Description
1.	E_{tot}	E_{tot}^*	Maximum stored energy over period T .
2.	f_{res}	f_{res}^*	Resonance frequency of the LCL filter.
3.	THD_{i_i}	$\text{THD}_{i_i}^*$	Total harmonic distortion of the current i_i .
4.	THD_{i_g}	$\text{THD}_{i_g}^*$	Total harmonic distortion of the current i_g .
5.	$\text{THD}_{u_{C_f}}$	$\text{THD}_{u_{C_f}}^*$	Total harmonic distortion of the voltage u_{C_f} .
6.	PF_g	PF_g^*	Power factor on the grid-side.
7.	P_g	P_g^*	Active power on the grid-side.

The instantaneous total energy of the system $E_{\text{tot}}(t)$ is described by:

$$E_{\text{tot}}(t) = \frac{1}{2}L_i i_i(t) + \frac{1}{2}L_g i_g(t)^2 + \frac{1}{2}C_f u_{C_f}(t), \quad (38)$$

which serves for the purpose of minimizing the physical components L_i , L_g , and C_f of the LCL filter [4]. Applying $E_{\text{tot}} = \text{argmax}_{t \in T}(E_{\text{tot}}(t))$ yields to the sought out instantaneous maximum stored energy in the LCL filter. The second characteristic is the LCL filter's resonance frequency f_{res} , which is described by Equation (11) introduced earlier in Section 2.1. The remaining characteristics are obtained by computing Fast Fourier Transform (FFT), such that: $\mathbf{Z}_{i_i} \leftarrow \text{FFT}(\mathbf{i}_i)$, $\mathbf{Z}_{i_g} \leftarrow \text{FFT}(\mathbf{i}_g)$, and $\mathbf{Z}_{u_{C_f}} \leftarrow \text{FFT}(\mathbf{u}_{C_f})$, where \mathbf{i}_i , \mathbf{i}_g , and \mathbf{u}_{C_f} are the outputs from Algorithm 6. Now, further computations from the complex FFT representations of \mathbf{Z}_{i_i} , \mathbf{Z}_{i_g} , and $\mathbf{Z}_{u_{C_f}}$ can be conducted. Multiplying Equation (4) from Section 2.1 with 100% and applying it to the input signals i_i , i_g , and u_{C_f} – the respective THD measures: THD_{i_i} , THD_{i_g} , and $\text{THD}_{u_{C_f}}$ are obtained. The harmonic content upper bound

parameter H may be selected freely, as long as, $H \geq 2$. One way of deriving the grid-side measures for PF_g and P_g from the complex FFT representation involves calculating the complex power \mathbf{s} described by:

$$\mathbf{s} = \frac{1}{2} \mathbf{u} \mathbf{i}^* = P + jQ, \quad (39)$$

where \mathbf{u} is the phasor voltage, and \mathbf{i}^* is the complex conjugate of the phasor current [28]. Equation (39) can also be written in terms of the real part P (active power) and the imaginary part Q (reactive power). Consequently, taking the real part from Equation (39) yields the grid-side active power $P_g = \text{Re}(\mathbf{s})$. The grid-side power factor PF_g is obtained by dividing the active power P_g by the apparent power $|\mathbf{s}|$ as:

$$\text{PF}_g = \frac{P_g}{|\mathbf{s}|}, \quad (40)$$

yielding the measure for the remaining performance characteristic [18]. The previously introduced performance characteristics can now be collected into vector:

$$\mathbf{p}_{\text{est}} = [E_{\text{tot}}, f_{\text{res}}, \text{THD}_{i_i}, \text{THD}_{i_g}, \text{THD}_{u_{C_f}}, \text{PF}_g, P_g], \quad (41)$$

which are computed for each design parameter state-vector candidate $\mathbf{x}^{(k)}$ whereas the elements of \mathbf{p}_{ref} are the predetermined objectives

$$\mathbf{p}_{\text{ref}} = [E_{\text{tot}}^*, f_{\text{res}}^*, \text{THD}_{i_i}^*, \text{THD}_{i_g}^*, \text{THD}_{u_{C_f}}^*, \text{PF}_g^*, P_g^*]. \quad (42)$$

3.4 Differential evolution optimisation

Recalling from Section 2 the two common approaches in identifying LCL design parameters, namely, iterative and optimising. In this work the latter approach has been adopted. For this approach to work, a global optimisation method capable of searching through a D -dimensional, potentially non-linear and non-differentiable, space will be required. Considering optimisation methods that utilize some kind of an objective function F_{obj} to steer the search, there are a number different strategies available, such as: Genetic Algorithm (GA), Evolution Strategies (ES), or Simulated Annealing (SA) based to mention a few [29, 30].

Example of an evolution based optimisation method, influenced by GA and ES methods, is the DE by Storn *et al.* [29]. It can be characterized as a stochastic parallel direct search method with an associated objective function F_{obj} , which may either be minimized or

maximized in a predetermined search space $\Omega[\mathbf{x}^L, \mathbf{x}^U]$ with respect to the parameter vector $\mathbf{x}^{(k)}$, such that $\mathbf{x}^{(k)} \in \Omega[\mathbf{x}^L, \mathbf{x}^U]$, where k is the k^{th} iteration, or generation, of the algorithm whereas \mathbf{x}^L and \mathbf{x}^U are lower and upper boundaries of the search space [29]. This is a characteristic that the DE has – emphasized by the four design requirements for the DE method by Storn *et al.* [29], which namely are:

1. Capability to address non-differentiable, non-linear and multimodal objective functions.
2. Parallelization of computation intensive objective functions.
3. Ease of use through the minimization of the number of control variables.
4. Good convergence characteristics.

There are several variant of the DE algorithm, where the algorithm differs on the mutation strategy, the number of difference vectors, and crossover scheme [29]. Here, only the standard implementation DE/rand/1/bin will be introduced, where 'rand' is referring to the principle of choosing randomly selected population vector for mutation, '1' is referring to the number of difference vectors, and finally 'bin' to the crossover scheme of independent binomial experiments [29]. Assuming now the DE/rand/1/bin variant, the algorithm starts by preparing an initial and randomly chosen D -dimensional population $\mathbf{x}_{i,j}^{(k)}$, where $i = 1, 2, \dots, N_p$, $j = 1, 2, \dots, D$, and $N_p, N_p \geq 4$ is the size of the population. This is followed by $k = 1, 2, \dots, N_g$ iterations over the population, where N_g is the maximum number of generations, such that: *mutation*, *crossover* and *selection* operations are applied for each generation k . For each population member $\mathbf{x}_{i,j}^{(k)}$, $i = 1, 2, \dots, N_p$, generate a mutated vector:

$$\mathbf{v}_{i,j}^{(k)} = \mathbf{x}_{r_1,j}^{(k)} + F[\mathbf{x}_{r_2,j}^{(k)} - \mathbf{x}_{r_3,j}^{(k)}], \quad (43)$$

where $F \in (0, 2]$ is a constant for controlling the amplification of the differential variation and $r_1, r_2, r_3 \in \{1, 2, \dots, N_p\}$ randomly chosen donor vectors from the population. Next, inside the same iteration, *crossover* is applied to introduce diversity to the perturbed trial vector $\mathbf{u}_{i,j}^{(k)}$:

$$\mathbf{u}_{i,j}^{(k)} = \begin{cases} \mathbf{v}_{i,j}^{(k)} & \text{if } p_{\text{Cr}} \leq U(0, 1)_{\mathbb{R}^+} \text{ or } j = j_{\text{rand}}, \\ \mathbf{x}_{i,j}^{(k)} & \text{otherwise,} \end{cases} \quad (44)$$

where p_{Cr} is the probability of *crossover*, uniform distribution $U(0, 1)_{\mathbb{R}^+}$ draw, and j_{rand} random number drawn from $U(0, 1)_{\mathbb{N}^+}$. Finally, the algorithm conducts *selection* whether or not i^{th} trial vector $\mathbf{u}_{i,j}^{(k)}$ replaces the respective target vector $\mathbf{x}_{i,j}^{(k)}$ using greedy selection. An adapted version of the DE/rand/1/bin is summarized in Algorithm 7 [29].

Algorithm 7 Differential evolution (DE/rand/1/bin).

Input:

F_{obj} = Objective function.

\mathbf{x}^L = Lower bound D -dimensional vector of the search space $\Omega[\mathbf{x}^L, \mathbf{x}^U]$.

\mathbf{x}^U = Upper bound D -dimensional vector of the search space $\Omega[\mathbf{x}^L, \mathbf{x}^U]$.

N_p = Size of the population to produce, $N_p \geq 4$.

N_g = Maximum number of generations to produce.

p_{Cr} = Crossover probability constant, $p_{\text{Cr}} \in (0, 1]$.

F = Differential variation amplification constant, $F \in (0, 2]$.

Output:

$\mathbf{x}_{i,:}^{(k)}$ = Vector of parameters for each population member $i \in \{1, 2, \dots, N_p\}$.

$\mathbf{x}_{\text{obj},i}^{(k)}$ = Vector of F_{obj} values for each population member $i \in \{1, 2, \dots, N_p\}$.

1. Initialize population $\mathbf{x}_{i,:}^{(1)} \in \Omega[\mathbf{x}^L, \mathbf{x}^U]$, $i \in \{1, 2, \dots, N_p\}$ with random values and set:

$$\mathbf{u}_{i,:}^{(1)} \leftarrow \mathbf{x}_{i,:}^{(1)}, \mathbf{x}_{\text{obj},i}^{(1)} \leftarrow F_{\text{obj}}(\mathbf{x}_{i,:}^{(1)}).$$

2. For each generation $k \in \{1, 2, \dots, N_g\}$:

For each population member $i \in \{1, 2, \dots, N_p\}$:

Generation

$$r_1 \leftarrow U(1, N_p)_{\mathbb{N}^+}, r_2 \leftarrow U(1, N_p)_{\mathbb{N}^+}, r_3 \leftarrow U(1, N_p)_{\mathbb{N}^+}, r_1 \neq r_2 \neq r_3 \neq i$$

Mutation

$$\mathbf{v}_{i,:}^{(k)} \leftarrow \mathbf{x}_{r_1,:}^{(k)} + F[\mathbf{x}_{r_2,:}^{(k)} - \mathbf{x}_{r_3,:}^{(k)}]$$

Crossover

$$j_{\text{rand}} \leftarrow U(1, D)_{\mathbb{N}^+}$$

For each dimension $j \in \{1, 2, \dots, D\}$:

$$p_{\text{Cr}} \leftarrow U(0, 1)_{\mathbb{R}^+}$$

if $p_{\text{Cr}} \leq j_{\text{rand}}$ **or** $j = j_{\text{rand}}$ **then**

Accept crossover

$$\mathbf{u}_{i,j}^{(k)} \leftarrow \max(\mathbf{x}^L, \min(\mathbf{v}_{i,j}^{(k)}, \mathbf{x}^U))$$

else

Reject crossover

$$\mathbf{u}_{i,j}^{(k)} \leftarrow \mathbf{x}_{i,j}^{(k)}$$

end

Selection

$$\mathbf{u}_{\text{obj},i}^{(k)} \leftarrow F_{\text{obj}}(\mathbf{u}_{i,:}^{(k)})$$

if $\mathbf{u}_{\text{obj},i}^{(k)} \leq \mathbf{x}_{\text{obj},i}^{(k)}$ **then**

$$\mathbf{x}_{i,:}^{(k)} \leftarrow \mathbf{u}_{i,:}^{(k)}$$

$$\mathbf{x}_{\text{obj},i}^{(k)} \leftarrow \mathbf{u}_{\text{obj},i}^{(k)}$$

end.

3. Finally, return the outputs:

$$\mathbf{x}_{i,:}^{(k)}, \mathbf{x}_{\text{obj},i}^{(k)}$$

4 EXPERIMENTS

In this section the conducted experiments shall be described and presented. This begins by explaining the practical experimental work conducted on VSI-model, LCL-model, performance characteristics, DE global optimisation method, and the results when the aforementioned are integrated together. This section will be addressing the two last objectives from Section 1 that, namely, were:

- Construction of the simulation environment with the models (Objective 5).
- Feasibility of the DE candidate solutions with respect to the selected performance characteristics (Objective 6).

The Section 4 is broken down to Subsections 4.1, 4.2, 4.3, and 4.4 for the detailed treatment of validation of the models, performance characteristics, objective function, and DE solution candidates derived by the proposed method.

4.1 Environment and models

In order to validate the VSI- and LCL-models, a specialised simulation environment is required. To this end, the author of this work chose to implement the relevant models and algorithms in MATLAB environment due to its wide adoption in academia and industry alike. It was also a conscious design decision to implement everything as either plain text MATLAB functions or scripts, and consequently, all the algorithms presented in Section 3 were handcrafted manually as code. Consequently, by having everything implemented as plain text code, there are no dependencies to any graphical programming environments such as *Simulink*, which is also a tool available from the same company providing the MATLAB programming environment. For the purpose of implementing the discontinuous SPWM switching function $s_x(t)$, $x \in \{a, b, c\}$ it shall be defined as in Equation (45):

$$s_x(t) = \begin{cases} 0 & \text{if } F_{0,x}(t) < C_x(\omega_{c,x}t), \\ 1 & \text{otherwise,} \end{cases} \quad (45)$$

where $F_{0,x}(t)$, $x \in \{a, b, c\}$ is the fundamental wave and $C_x(\omega_{c,x}t)$, $C_x \in \{\text{sawtooth, triangle}\}$, $x \in \{a, b, c\}$ is the carrier wave generator function with angular frequency $\omega_{c,x}$, $x \in \{a, b, c\}$, for all evaluation steps t . $F_{0,x}(t)$ corresponds to $F_0(t)$ in Equation (34) with fundamental

wave period T_0 and $\omega_{c,x}$ is the angular frequency of the carrier wave similar to ω_0 in Equation (33), but with period T_c . A dedicated test script was devised for the validation of the SPWM switching function implementation. The objective of this test script was to plot the switching function $s_x(t)$ output waveforms with the given input parameters. These input parameters are listed in Table 2. The phase-shifted discontinuous SPWM switching

Table 2. SPWM test input parameters.

Parameter	Value	Unit	Description
u_{dc}	750	VDC	Fixed VSI-side DC-link voltage.
T_0	0.20	s	Fundamental wave period.
θ_0	0.00	rad	Fundamental wave phase-shift.
T_c	0.01	s	Carrier wave period.
θ_c	0.00	rad	Carrier wave phase-shift.
m_a	0.90	-	Modulation amplitude.
C_x	sawtooth	-	Carrier generator function.

functions for each phase a three-phase two-level VSI can be easily derived from Equations (34) and (45) by setting $\theta_0 \in \{0, \frac{2}{3}\pi, \frac{4}{3}\pi\}$ for $x \in \{a, b, c\}$. However, this shall not be covered in further detail here. The resulting plot for a single switching function $s_x(t)$ given the parameters from Table 2 for $C_x \in \{\text{sawtooth}, \text{triangle}\}$ is depicted in Figure 7. Next,

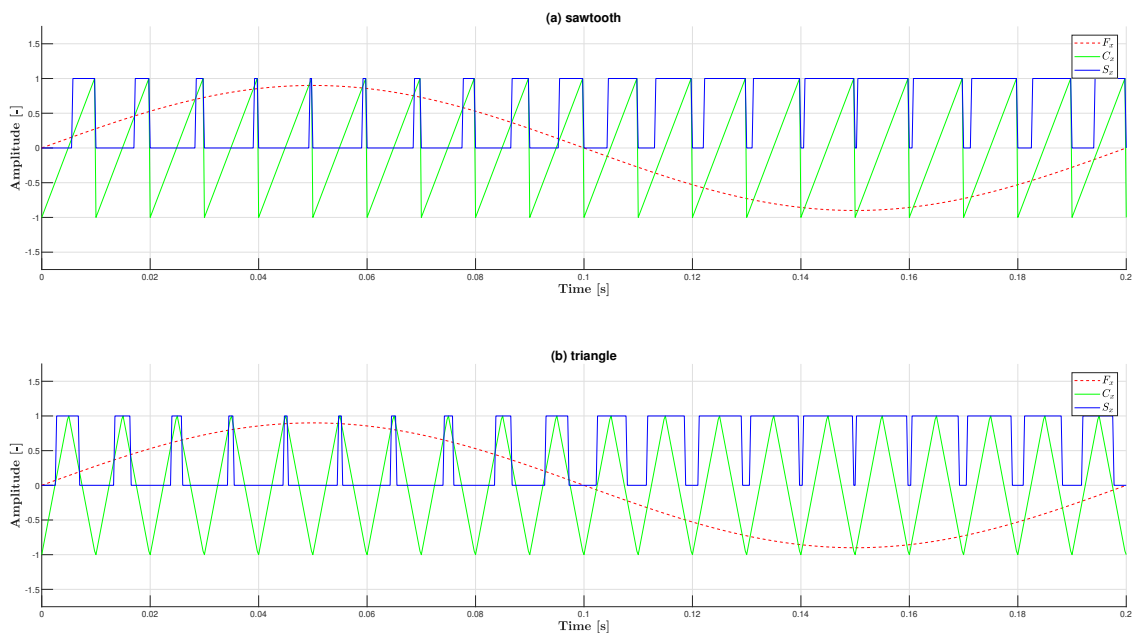


Figure 7. Single phase SPWM switching with carrier generator function; (a) sawtooth; (b) triangle.

applying the output of Equation (45) into Equation (29) from Section 3.1 for a fixed DC-link voltage u_{dc} (750V) the output voltage of the top switches T_1 , T_3 , and T_5 with respect to neutral z from Figure 6 can be computed. Similarly for the bottom switches T_4 , T_6 , and T_2 , which leads to SPWM voltage switching pattern depicted in Figure 8 for one phase, where the SPWM switching pattern is from $u_{dc}-$ (bottom: $-750V$) to $u_{dc}+$ (top: $+750V$). Having the SPWM switching and the respective voltage output generation in place there

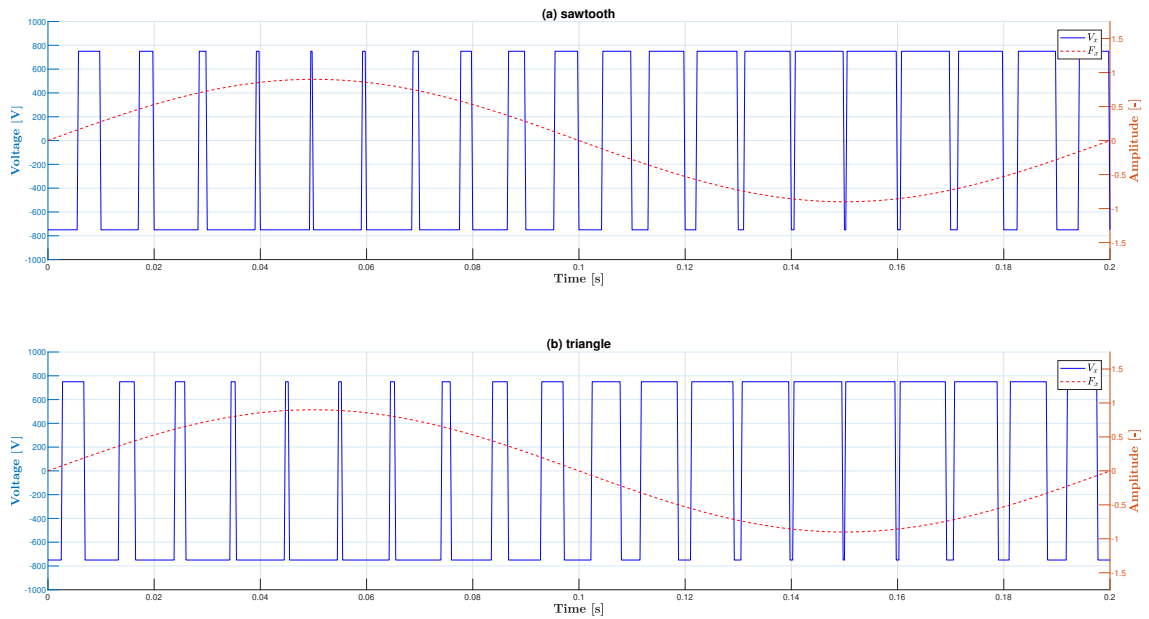


Figure 8. Single phase SPWM voltage with carrier generator function; (a) sawtooth; (b) triangle.

is now a simple model of the VSI as well. The next step is to feed the voltage output from the VSI-model into the LCL-model, which numerically integrates the electrical quantities i_i , i_g , and u_{C_f} as an output to the given initial conditions and input parameters described in Algorithm 6 in Section 3.2. For the validation of Algorithm 6 implementation, again, a dedicated test script was devised to analyse the output of the numerical LCL ODE solver. Two alternative numerical ODE solver approaches were tested: Forward-Euler (FE) and fourth-order RK described in Algorithm 6. Both algorithms were subjected to the same simulation parameters listed in Table 3.

The corresponding known LCL filter design parameters from the results of Reznik *et al.* [1] are summarized in Table 4. With the chosen input values from Tables 3 and 4 the algorithms produced the output depicted in Figure A1.1 of Appendix 1, where in Figure A1.1a is a plot of the computed i_i and i_g currents using FE method and, respectively, in Figure A1.1b for the fourth-order RK. FFT frequency spectrum magnitude plots in for i_i and i_g using FE are denoted in Figures A1.1c and A1.1e, where as for the fourth-order

Table 3. ODE solver simulation parameters.

Parameter	Value	Unit	Description
K	5	-	Number of fundamental wave period cycles to compute.
u_g	120	VAC	Grid-side phase RMS voltage.
u_{dc}	400	VDC	VSI-side DC-link voltage.
T_0	16.70	ms	Fundamental wave period, equivalent to $f_g = 60$ Hz.
θ_0	0.00	rad	Fundamental wave phase-shift, equivalent to 0° .
T_c	250.00	μs	Carrier wave period, equivalent to $f_{sw} = 4000$ Hz.
θ_c	0.00	rad	Carrier wave phase-shift, corresponds to 0° .
T_s	45.45	μs	Sampling period, corresponds to $f_s = 22000$ Hz.
m_a	0.50	-	Modulation amplitude.
C_x	sawtooth	-	Carrier generator method, sawtooth.

Table 4. ODE solver LCL filter design parameters by Reznik *et al.* [1].

L_i [mH]	R_i [Ω]	C_f [μF]	R_d [Ω]	L_g [mH]	R_g [Ω]
2.23	1.00	15.00	0.55	0.05	1.00

RK in Figures A1.1d and A1.1f with the three most significant harmonic components $k \in \{1, 2, 3\}$ excluding the 0th DC-offset component. Observing at the graphs in Figure A1.1 it implies RK being numerically more stable, and thus, being the better choice. However, concrete numerical evidence of this was required. For this purpose, the THD metrics were computed from the FFT complex representations of the i_i , i_g , and u_{C_f} electrical quantities, such that the numerical solution performance of FE and RK methods could be quantitatively compared. The results of this comparison, with the respective input parameters from Table 3, are presented in Table 5. While the fourth-order RK produces

Table 5. THD comparison between FE and fourth-order RK ODE solvers.

Characteristic	FE [%]	RK [%]	Δ [%pt]
THD $_{i_i}$	5.21	5.22	0.01
THD $_{i_g}$	7.84	5.63	2.21
THD $_{u_{C_f}}$	26.29	16.78	9.51

slightly higher THD $_{i_i}$ than FE, thus implying slightly higher harmonic distortion for i_i , but it does outperform for THD $_{i_g}$ and THD $_{u_{C_f}}$. This implies lesser harmonic distortion in the solutions of i_g and u_{C_f} while adding to the argument of selecting the fourth-order RK as the LCL ODE solver. Given the evidence from the experimentation, the fourth-order

RK method was consequently chosen as the numerical LCL ODE solver method for this work.

4.2 Characteristics

The computation of the performance characteristics listed in Table 1 of Section 3.3 can be divided in two categories, where the computation is either a direct implementation of an equation or something that is required to be derived from FFT complex representation of specific electrical quantities. Examples of the former are E_{tot} and f_{res} quantities, which can be directly computed from Equations (11) and (38) given the $\mathbf{x}^{(k)}$ design parameter candidates and the solved electrical quantities from Algorithm 6. The remaining characteristics requiring FFT complex representations for further computations, namely, are: THD_{i_i} , THD_{i_g} , $\text{THD}_{u_{C_f}}$, PF_g , and P_g . Merging these conditions with the already known electrical quantities of i_i , i_g , and u_g a procedure for computing the performance characteristics can be derived, which is described in Algorithm 8. The validation of the performance characteristics was conducted similarly to the VSI, LCL, and ODE models by implementing a dedicated test script running through predefined test scenarios. However, in the interest of compactness these test scenarios will not be explored further in this work's context.

4.3 Objective function

In Section 3.4 Algorithm 7 the principle of DE/rand/1/bin global optimisation search method was described, but the details of the objective function F_{obj} were omitted. Building up to the implementation details of the objective function F_{obj} it should be first noted that the typical setting for the objective function is either minimization or maximization of its value. Depending on the underlying problem the objective can, for example in a financial setting, be the minimization of cost or maximization of profit. Recalling from Section 2 that there are existing LCL design parameter identification methods, where the target is to minimize the error, that is cost, of the candidate solution with respect predetermined design targets. Consequently, minimization of cost function based approach was chosen here as well. In this context the objective will be to minimize the error of the estimated performance characteristics \mathbf{p}_{est} with respect to the target \mathbf{p}_{ref} given candidate parameters $\mathbf{x}^{(k)}$.

Algorithm 8 Computation of the performance characteristics (perfchr).

Input:

$\mathbf{x}^{(k)}$ = Input parameters of the k^{th} evaluation of the objective function.

\mathbf{i}_i = Vector of VSI-side phase current i_i observed at times $\mathbf{t}_{1:T}$.

\mathbf{i}_g = Vector of grid-side phase current i_g observed at times $\mathbf{t}_{1:T}$.

\mathbf{u}_{C_f} = Vector of filter capacitor voltage u_{C_f} observed at times $\mathbf{t}_{1:T}$.

u_g = Grid-side phase voltage function.

Output:

\mathbf{p}_{est} = Vector of performance characteristics with respect to $\mathbf{x}^{(k)}$.

1. Decompose parameter vector $\mathbf{x}^{(k)}$:

$$L_i \leftarrow \mathbf{x}_1^{(k)}, R_i \leftarrow \mathbf{x}_2^{(k)}, C_f \leftarrow \mathbf{x}_3^{(k)}, R_d \leftarrow \mathbf{x}_4^{(k)}, L_g \leftarrow \mathbf{x}_5^{(k)}, R_g \leftarrow \mathbf{x}_6^{(k)}.$$

2. Compute E_{tot} and f_{res} values:

$$E_{\text{tot}} \leftarrow \max\left(\frac{1}{2}L_i\mathbf{i}_i^2 + \frac{1}{2}L_g\mathbf{i}_g^2 + \frac{1}{2}C_f\mathbf{u}_{C_f}\right), f_{\text{res}} \leftarrow \sqrt{\frac{L_i+L_g}{L_iL_gC_f}}.$$

3. Compute the FFT's, such that:

$$\mathbf{Z}_{i_i} \leftarrow \text{FFT}(\mathbf{i}_i), \mathbf{Z}_{i_g} \leftarrow \text{FFT}(\mathbf{i}_g), \mathbf{Z}_{u_{C_f}} \leftarrow \text{FFT}(\mathbf{u}_{C_f}).$$

4. Compute the THD values:

$$\text{THD}_{i_i} \leftarrow \text{THD}(\mathbf{Z}_{i_i}), \text{THD}_{i_g} \leftarrow \text{THD}(\mathbf{Z}_{i_g}), \text{THD}_{u_{C_f}} \leftarrow \text{THD}(\mathbf{Z}_{u_{C_f}}).$$

5. Compute the grid-side power factor and active power:

$$\text{PF}_g \leftarrow \text{PF}(\mathbf{Z}_{i_g}, \mathbf{Z}_{u_g}), P_g \leftarrow \text{P}(\mathbf{Z}_{i_g}, \mathbf{Z}_{u_g}).$$

6. Compose the \mathbf{p}_{est} vector and return:

$$\mathbf{p}_{\text{est}} \leftarrow [E_{\text{tot}}, f_{\text{res}}, \text{THD}_{i_i}, \text{THD}_{i_g}, \text{THD}_{u_{C_f}}, \text{PF}_g, P_g].$$

Several alternative ways of realizing the cost evaluation were considered, such as: linear error, squared error, and desirability functions. During the practical implementation phase of the simulation environment all of these were experimented with. However, the author of this work opted to used one-sided and two-sided desirability functions due to their flexibility. For each performance characteristic estimate $\mathbf{p}_{\text{est},i}$, where i is the i^{th} performance characteristics, the respective desirability function is parametrised accordingly with the performance target $\mathbf{p}_{\text{ref},i}$. The chosen one-sided desirability function is described in Equation (46):

$$\text{onesided}(y, r_1, \cdot, L, T) = \begin{cases} 0 & y < L, \\ \left(\frac{y-L}{T-L}\right)^{r_1} & L \leq y \leq T, \\ 1 & y > T, \end{cases} \quad (46)$$

where y is the input value, r_1 is the weight, \cdot denoting an unused input value, L being the

lower bound, and T being the target [31]. Choosing the weight $r_1 = 1$, the function is linear. However, if $r_1 > 1$ more weight is being placed to be closer to the target T , and conversely if $0 < r_1 < 1$ less weight, when approaching from the lower bound side of the target T . Similarly to the one-sided in Equation (46) the definition of the two-sided is denoted in Equation (47):

$$\text{twosided}(y, r_1, r_2, L, T) = \begin{cases} 0 & y < L, \\ \left(\frac{y-L}{T-L}\right)^{r_1} & L \leq y \leq T, \\ \left(\frac{U-y}{U-T}\right)^{r_2} & T \leq y \leq U, \\ 0 & y > U, \end{cases} \quad (47)$$

where r_2 is weight of the desirability function when target T is being approached from the upper bound side [31]. Now, utilizing the results from Equations (46) and (47) the final cost function can be composed from each performance characteristic passed through the respective desirability function d_i , such that:

$$\text{costfunc}(\mathbf{p}_{\text{est}}, \mathbf{r}_1, \mathbf{r}_2, \mathbf{p}_{\text{ref}}^L, \mathbf{p}_{\text{ref}}, \mathbf{p}_{\text{ref}}^U) = - \sum_{i=1}^N d_i(\mathbf{p}_{\text{est},i}, \mathbf{r}_{1,i}, \mathbf{r}_{2,i}, \mathbf{p}_{\text{ref},i}^L, \mathbf{p}_{\text{ref},i}, \mathbf{p}_{\text{ref},i}^U), \quad (48)$$

where N is the number of desirability functions, \mathbf{r}_1 and \mathbf{r}_2 are vectors of weights; while $\mathbf{p}_{\text{ref}}^L$ and $\mathbf{p}_{\text{ref}}^U$ are the lower and upper bounds of the target areas in desirability functions d_i , $i \in \{1, 2, \dots, N\}$. Combining the result of Equation (48) with Algorithms 6 and 8 the resulting objective function F_{obj} can be formalized. This is described in Algorithm 9, where F_{obj} is now being called by Algorithm 7 for each trial solution $i \in \{1, 2, \dots, N_p\}$ of the k^{th} DE generation. The number of LCL ODE solution evaluation steps is governed by the K number cycles of the fundamental period T_0 , where the number of time steps is denoted by the size $|KT_0|$. The $\mathbf{p}_{\text{ref}}^L$, \mathbf{p}_{ref} , and $\mathbf{p}_{\text{ref}}^U$ inputs in Algorithm 9 are captured as a closure, such that $F_{\text{obj}}(\cdot) := F_{\text{obj}}(\cdot, \mathbf{p}_{\text{ref}}^L, \mathbf{p}_{\text{ref}}, \mathbf{p}_{\text{ref}}^U)$ prior to passing the F_{obj} is as an input to Algorithm 7. Thus, providing a compatible interface for passing in a solution candidate parameter input vector $\mathbf{x}^{(k)}$ for each population candidate in the current generation.

4.4 Solution candidates

Now, all necessary the groundwork has been laid out to conduct experiments on identifying LCL filter design parameters with the proposed methods utilizing the DE global optimisation method. To be able to conduct the experiments it was important to identify the reasonable performance targets for the respective desirability function parameters of the

Algorithm 9 Objective function used in conjunction with DE/rand/1/bin (F_{obj}).

Input:

$\mathbf{x}^{(k)}$ = Input parameters of the k^{th} evaluation of the objective function.

$\mathbf{p}_{\text{ref}}^L$ = Lower bounds of the targeted performance area.

\mathbf{p}_{ref} = Targeted performance of the solution.

$\mathbf{p}_{\text{ref}}^U$ = Upper bounds of the targeted performance area.

Output:

C = Evaluated objective function value with the given $\mathbf{x}^{(k)}$ input parameters.

1. Setup evaluation parameters, such that:

$K \leftarrow$ number of fundamental wave cycles to compute,

$T_0 \leftarrow$ fundamental wave period in seconds,

$T_c \leftarrow$ carrier wave period in seconds,

$T_s \leftarrow$ SPWM switching period in seconds,

$\mathbf{u} \leftarrow$ VSI- and grid-side voltage functions $[u_i, u_g]$,

$\mathbf{x}^{(0)} \leftarrow$ LCL ODE initial conditions,

$\mathbf{p} \leftarrow$ LCL ODE model parameters,

$\mathbf{r}_1 \leftarrow$ first set of weights for the cost function,

$\mathbf{r}_2 \leftarrow$ second set of weights for the cost function, and

$\mathbf{t} \leftarrow$ LCL ODE solution evaluation time steps $\mathbf{t}_i, i \in \{1, 2, \dots, |KT_0|\}$.

2. Solve the LCL ODE model:

$[\mathbf{i}_i, \mathbf{i}_g, \mathbf{u}_{C_f}] \leftarrow \text{lcloderk4}(\mathbf{t}, \mathbf{x}^{(0)}, \mathbf{u}, \mathbf{p})$.

3. Compute performance characteristics:

$\mathbf{p}_{\text{est}} \leftarrow \text{perfchr}(\mathbf{x}^{(k)}, \mathbf{i}_i, \mathbf{i}_g, \mathbf{u}_{C_f}, u_g)$.

4. Evaluate the cost function and return:

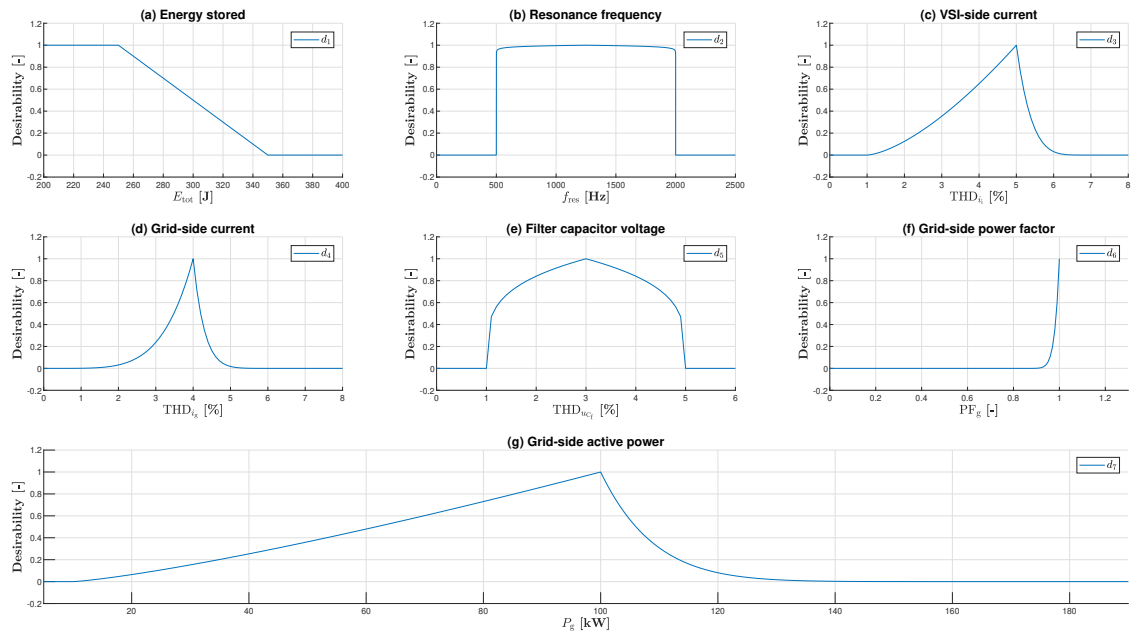
$C \leftarrow \text{costfunc}(\mathbf{p}_{\text{est}}, \mathbf{r}_1, \mathbf{r}_2, \mathbf{p}_{\text{ref}}^L, \mathbf{p}_{\text{ref}}, \mathbf{p}_{\text{ref}}^U)$.

cost function (costfunc). For this purpose, there needed to be many manually conducted trial runs of the whole optimisation procedure, to come up with reasonable desirability function parameters. Choosing too narrow or constraining parameters for the desirability functions d_i may lead to poor overall convergence where the search is not capturing good solutions with respect to some performance characteristic. To this end, the corresponding desirability functions d_i with respect to $\mathbf{p}_{\text{ref},i}$ performance characteristic targets are listed in Table 6, where \mathbf{T}_i is the i^{th} target value with \mathbf{L}_i and \mathbf{U}_i being the lower and upper limits accordingly.

Plotting each of the desirability functions d_i with the respective parameters $\mathbf{r}_{1,i}$, $\mathbf{r}_{2,i}$, \mathbf{L}_i , \mathbf{T}_i , and \mathbf{U}_i from Table 6 it yields to Figure 9. Now, having the optimisation target and desirability function parameters in place it is time to focus on the simulation environment parameters. These are the parameters needed to run the contents of the objective function

Table 6. Performance characteristic targets for the DE global optimisation search.

i	Characteristic d_i	$\mathbf{r}_{1,i}$	$\mathbf{r}_{2,i}$	\mathbf{L}_i	\mathbf{T}_i	\mathbf{U}_i	Unit
1	E_{tot}	1.00	-	250.00	255.00	350.00	J
2	f_{res}	0.01	0.01	500.00	1250.00	2000.00	Hz
3	THD_{i_i}	1.50	5.00	1.00	5.00	7.00	%
4	THD_{i_g}	5.00	10.00	0.00	4.00	7.00	%
5	$\text{THD}_{u_{C_f}}$	0.25	0.25	1.00	2.00	5.00	%
6	PF_g	7.50	-	0.80	1.00	1.00	-
7	P_g	1.25	15.00	10.00	100.00	190.00	kW

**Figure 9.** Desirability functions: (a) instantaneous energy stored E_{tot} ; (b) resonance frequency f_{res} ; (c) VSI-side current THD_{i_i} ; (d) grid-side current THD_{i_g} ; (e) filter capacitor voltage $\text{THD}_{u_{C_f}}$; (f) grid-side power factor PF_g ; (g) grid-side active power P_g .

F_{obj} , thus excluding the design bounds and differential evolution process parameters. The simulation environment parameters used in the subsequent experiments are summarized in Table 7.

Denoting the sets of the design parameter bounds as: $\mathbf{x}^L \in \{L_i^L, R_i^L, C_f^L, R_d^L, L_g^L, R_g^L\}$ for the lower and $\mathbf{x}^U \in \{L_i^U, R_i^U, C_f^U, R_d^U, L_g^U, R_g^U\}$ upper bounds – the limits of the design parameter search space $\Omega[\mathbf{x}^L, \mathbf{x}^U]$ were set as in Table 8. The remaining set of parameters that have been not yet introduced are for controlling the differential evolution optimisation process behaviour. Namely, these are the crossover probability C_r , mutation scaling factor F , population size N_p , and the maximum number of generations N_g to produce during the

Table 7. Simulation environment parameters.

Parameter	Value	Unit	Description
K	5	-	Number of fundamental wave period cycles to compute.
u_g	230	VAC	Grid-side phase RMS voltage.
u_{dc}	750	VDC	VSI-side DC-link voltage.
T_0	20.00	ms	Fundamental wave period, corresponds to $f_g = 50$ Hz.
θ_0	0.00	rad	Fundamental wave phase shift, corresponds to 0° .
T_c	250.00	μs	Carrier wave period, corresponds to $f_{sw} = 4000$ Hz.
θ_c	0.00	rad	Carrier wave phase-shift, corresponds to 0° .
T_s	45.45	μs	Sampling period, corresponds to $f_s = 22000$ Hz.
m_a	0.90	-	Modulation amplitude.
C_x	sawtooth	-	Carrier generator method, sawtooth.

Table 8. Design parameter search space $\Omega[\mathbf{x}^L, \mathbf{x}^U]$.

Parameter	\mathbf{x}_i^L	\mathbf{x}_i^U	Unit	Description
L_i	0.01	20.00	mH	VSI-side inductance.
R_i	0.01	5.00	Ω	VSI-side resistance.
C_f	1.00	550.00	μF	Filter capacitance.
R_d	0.01	10.00	Ω	Filter damping resistance.
L_g	0.01	3.00	mH	Grid-side inductance.
R_g	0.01	5.00	Ω	Grid-side resistance.

DE search. The DE global optimisation search experiments were, thus, conducted with the full simulation environment using the parameter values from the Tables 7, 8, and Table 9 below. With the parameters from Tables 7, 8, and 9 the DE global optimisation search

Table 9. Differential evolution parameters.

Parameter	Value	Description
N_p	100	Differential evolution population size.
C_r	0.90	Differential evolution crossover probability.
F	0.80	Mutation scaling factor.

was conducted with three different generation sizes $N_g^{(i)}$, $i \in \{1, 2, 3\}$ for a fixed population N_p , such that $N_p^{(1)} = 100$, $N_p^{(2)} = 300$, and $N_p^{(3)} = 900$. The progression of the objective function $F_{obj}^{(j)}$, $j \in \{1, 2, 3\}$ as a function of the number generations $N_g^{(i)}$ is depicted in Figure 10, where j is the j^{th} fittest solution in ascending order from the best to the next best. Clearly, the objective function value converges towards -7 value, which is the absolute

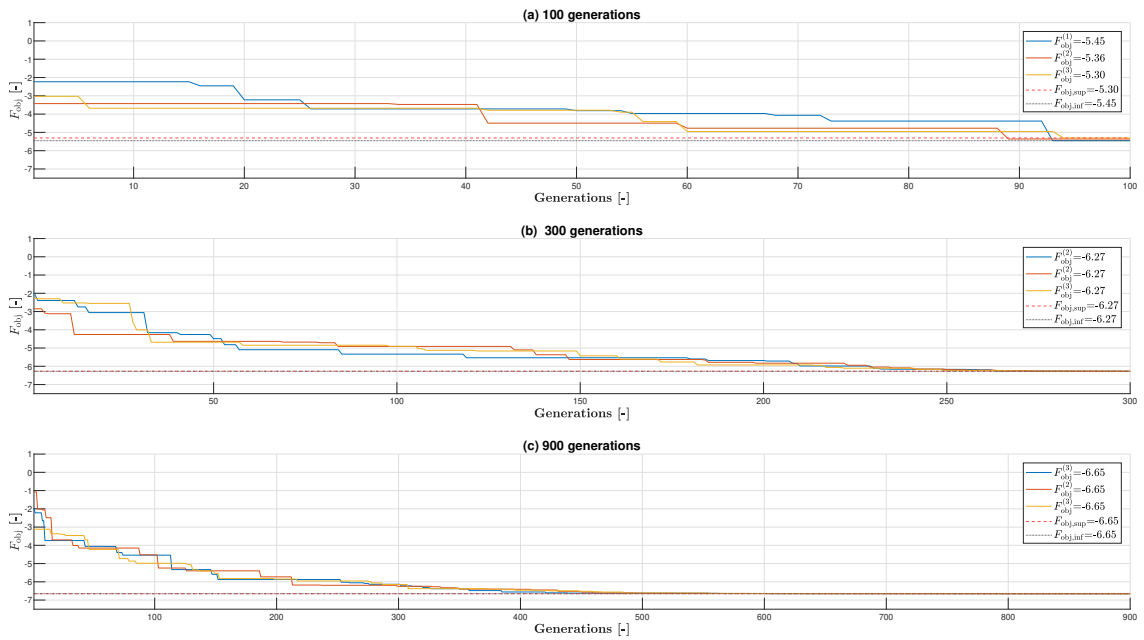


Figure 10. Objective function progression of three generation sizes: (a) $N_p^{(1)} = 100$; (b) $N_p^{(2)} = 300$; (c) $N_p^{(3)} = 900$.

minimum value that the cost function can achieve, as the number of generations increase. It is also evident that the cost function and performance characteristics approach the desired targets as the number of generations increase. The results of the three best solutions for each experiment i , $i \in \{1, 2, 3\}$ with the corresponding maximum number of generations and elapsed computation time $T_{elapsed}^{(i)}$, $i \in \{1, 2, 3\}$ are summarized in Table 10, such that the objective function value with the respective performance characteristic values are on the same row. The progression of the candidate solution is clearly visible from the plot comparing best solutions with maximum number of generations $N_g^{(i)}$, $i \in \{1, 2, 3\}$ for the electric output quantities: i_i , i_g , and u_{C_f} depicted in Figure A1.2 of Appendix 1.

Concluding with the DE search results of the LCL design parameter candidates with the three best F_{obj} values for each experimented number of maximum generations. The results are summarized in Table 11, where it can be witnessed, that the $F_{obj}^{(i)}$, $i \in \{1, 2, 3\}$ value tends toward the absolute minimum as the number of generations $N_g^{(i)}$, $i \in \{1, 2, 3\}$ increases. This implies convergence on the proposed method, which is supported by the observation, that there is no major decrease in the $F_{obj}^{(3)}$ value after 500 generations of the DE search. It is also worth pointing out the differences between the L_i and L_g inductance values in Table 11 for all candidate solutions, the L_i is having orders of magnitude higher inductance values. This makes sense as the VSI requires more conditioning due to its SPWM switching compared to the sinusoidal input waveform on the grid-side. The amount of the LCL filter capacitance C_f approaches its upper bound limit $550\mu F$ as the

Table 10. Top three candidate solutions and respective performance characteristics for $N_g^{(i)}$, $i \in \{1, 2, 3\}$.

i	F_{obj}	E_{tot} [J]	f_{res} [Hz]	THD_{i_i} [%]	THD_{i_g} [%]	$\text{THD}_{u_{c_f}}$ [%]	PF_g	P_g [kW]
$N_g^{(1)} = 100, T_{\text{elapsed}}^{(1)} = 164.94$ s								
1.	-5.45	104.24	725.55	4.07	4.01	1.98	0.99	30.57
2.	-5.36	127.19	718.22	3.95	3.93	1.98	0.99	36.31
3.	-5.30	73.66	1564.96	4.61	3.98	1.21	0.99	26.11
$N_g^{(2)} = 300, T_{\text{elapsed}}^{(2)} = 795.14$ s								
1.	-6.27	254.96	723.71	4.69	4.00	2.74	0.99	86.63
2.	-6.27	254.95	723.58	4.69	4.00	2.74	0.99	86.63
3.	-6.27	255.02	723.22	4.69	4.00	2.74	0.99	86.65
$N_g^{(3)} = 900, T_{\text{elapsed}}^{(3)} = 2284.01$ s								
1.	-6.65	255.01	1074.58	5.00	4.00	2.00	0.99	96.90
2.	-6.65	255.00	1074.31	5.00	4.00	2.00	0.99	96.90
3.	-6.65	254.99	1073.50	5.00	4.00	2.00	0.99	96.88

number of generations increase. The damping resistance R_d does not vary very much during the process, but ultimately settles near the lower bound limit of its search space. It is also worth recognising that in a real-world setting the resistances R_i and R_g are coming from the properties of the conductors rather than freely selectable. However, having a window for the both did improve the convergence of the proposed method.

Table 11. Top three design parameter candidates for each maximum number of generations $N_g^{(i)}$, $i \in \{1, 2, 3\}$.

i	L_i [mH]	R_i [Ω]	C_f [μF]	R_d [Ω]	L_g [mH]	R_g [Ω]
$N_g^{(1)} = 100$						
1.	3.61	4.30	258.46	0.01	0.20	0.01
2.	3.13	3.60	303.13	0.01	0.17	0.01
3.	3.73	5.00	179.77	0.08	0.06	0.13
$N_g^{(2)} = 300$						
1.	1.10	1.54	550.00	0.01	0.10	0.01
2.	1.10	1.54	550.00	0.01	0.10	0.01
3.	1.10	1.54	550.00	0.01	0.10	0.01
$N_g^{(3)} = 900$						
1.	0.92	1.38	549.64	0.03	0.04	0.01
2.	0.92	1.38	549.90	0.03	0.04	0.01
3.	0.92	1.38	548.99	0.03	0.04	0.01

5 DISCUSSION AND CONCLUSIONS

The topic of this work did pose an interesting challenge to find relevant equations, models, and algorithms to achieve the goal of addressing the research questions and objectives presented in Section 1. Considering prior work in the field, such as the ones explored in Section 2, an alternative numerical and computational LCL filter design parameter identification method was constructed. To address the research questions and goals posed in Section 1, relevant models and algorithms needed to be developed for a grid connected system with a PWM switched VSI device and a LCL filter. For the quantification of the system performance, with respect to the desired design targets, relevant performance characteristics needed to be identified as well. With the aforementioned characteristics, a global design parameter search method was selected, which in this work's scope was the DE global optimisation method. All relevant models and algorithms were introduced in Section 3. The implementation, experimentation and validation of the proposed methods were carried over in Section 4. Now, in this final section practical implementation, experimentation, and future improvement ideas shall be explored further.

Next, taking a reflection on the experiments conducted in Section 4 the first and foremost challenge was to develop simple, but effective PWM modulation method to emulate the behaviour of a VSI device. For this purpose SPWM method was selected (Algorithm 5), where basically the SPWM pulse train is generated by comparing fundamental wave to a carrier wave pattern by switching the output state at the intersections of the two waveforms. Having only to control the modulation amplitude m_a , fundamental wave period T_0 , fundamental wave phase-shift θ_0 , and carrier wave phase shift θ_c with an appropriate carrier waveform generation method, such as the sawtooth, this reasonably straightforward to realize. However, orders of more challenging task was to devise reliably working numerical ODE solver (Algorithm 6) to compute the state-space model of the grid-connected electrical system with LCL and VSI devices. Here, the research paper by Reznik *et al.* [1] proved to be a valuable source. After many experimentation's with FE and fourth-order RK numerical ODE solvers; the latter method was chosen due to its better numerical stability characteristics. This also allowed to use a longer time step length Δt compared to its rival, and yet, preventing the ODE solution from diverging to infinity.

After there was a stable and reliable method for solving the system under analysis, the objective was to develop performance characteristics that would capture the essential system behaviour. Here, the research papers from Liserre *et al.* [6] and Gurrola-Corral *et al.* [4] were the main sources from which the seven performance characteristics (Table 1) used in this work were derived. Two of the performance characteristics (E_{tot} , f_{res}) were

straightforward implementations of Equations (38) and (11). The rest required to compute FFT either from the known system input signals or from the output of the numerical LCL ODE model (Algorithm 8). The research paper by Storn *et al.* [29] was used as the primary source in the practical implementation of the DE method. This proved to be the most computationally intensive procedure. Namely, this was the product of how the DE global optimisation method works (Algorithm 7), where the objective function F_{obj} (Algorithm 9) is evaluated for each trial solution of the respective running generation. Clearly, here was the greatest improvement potential for future in terms of used computation time as implied by Table 10. This would be especially true if the number of performance goals \mathbf{p}_{ref} or the dimensions of the design parameters \mathbf{x} are increased. Ignoring the required computational time for the moment, the quality of the solution candidates did improve as the maximum number of generations $N_g^{(i)}$, $i \in \{1, 2, 3\}$ were increased, where $N_{g(3)}$ did yield the smallest F_{obj} value and best performance characteristics in Table 10 with the respective LCL filter design parameters in Table 11. For convenience, in Table A1.1 of Appendix 1 the reader may find the corresponding per-unit values for L_i , C_f , and L_g often used in electrical engineering. These were obtained by utilising Equations (1), (2), and (3) by dividing the respective component values from Table 11 with the base values. Encouragingly, the methods developed in this work did provide convergence (Figure 10) and progressive improvement in the quality of the solution (Figure A1.2) as the maximum number of DE generations was increased.

Over the course of this work, and especially during the work performed on the practical problem solving, it was evident that a number of improvement ideas for the future did come across. Starting with most obvious one, namely, the elapsed computation time. While the DE method can be written as parallelized algorithm in the chosen MATLAB programming environment the utilisation of, for example, Graphics Processing Unit (GPU) parallel computing capabilities could offer significant performance boost. This especially for the FFT computations, but also taking it further by assigning each trial solution of the respective generation as parallel computations. Of course, this would require diligent design work for synchronizing all the parallel computations in a fashion where the increased complexity of the implementation work does not outweigh its benefits. The second clear improvement would be to incorporate commercially available capacitor and resistor sizes in the design parameter search space $\Omega[\mathbf{x}^L, \mathbf{x}^U]$. In the scope of this work all of the LCL filter design parameters \mathbf{x} were considered to be continuous values over the search domain. However, this is not case in real world applications with most notably the capacitor (u_{C_f}) and resistor (R_i , R_d , and R_g) components. However, for the inductive components (L_i and L_g) there is more degrees-of-freedom to choose the values through the choice of core material, geometry, and number of turns in the component which may

be acquired by through suppliers of discrete or custom components. The third improvement is the addition of material cost of the LCL filter as for the industrial manufacturing companies the overall material cost of the product is a very essential design target. This is often due to competition in the market and the solutions. Being able to offer a competitive product with desired performance at low material and manufacturing cost level, is a significant competitive advantage to a company. The fourth and final improvement prospect is to extend the models and computations from single-phase models to three-phase models. This would improve the fidelity and accuracy of the simulation, where for example the capacitor voltage u_{C_f} should resemble closer to a constant value due to the three phases having a symmetric phase shift of 120° . Now, in Figures A1.2b, A1.2d, and A1.2f this is shown as sinusoidal waveform with an amplitude in the units of hundreds volts. Another source of simulation fidelity improvement would be to model the material and geometric properties of the inductive components. Of course these fidelity improvements would come with the cost of additional computation complexity and time, where the trade-offs would need to be carefully considered.

Finally, taking a reflection on the six objectives defined in Section 1, where the development of the mathematical models and methods for SPWM switched VSI, LCL filter, performance characteristics, and DE global optimisation search were introduced in Section 3, thus addressing the Objectives 1, 2, 3, and 4. In Section 4 the proposed methods were implemented and integrated to address the two remaining ones, namely, Objectives 5 and 6. While specific delimitations were placed in Section 1 on the scope of the work, based on the experiments and results from Section 4 the author of this work is inclined to make the statement that the proposed method can be a viable approach in an industrial setting as well. Notably, there would be some areas of improvement to be addressed, such as introduction of additional performance targets or increase in the dimensionality of the design parameters. However, these could be addressed with improvements on the parallelization of the computations and the underlying methods that the proposed method is built on. The choice of this work's topic was, to a degree, embedded with risk due to its blend over two engineering science domains with elements from *Electrical Engineering* coupled with solution methods from *Computational Engineering* proved to be a major challenge. However, considering the inherent uncertainty in the beginning this topic proved to be within the reach of the proposed methods, thus leading in to a favourable outcome in the end. To this end, the author of this work believes, that the objectives set out to this work were successfully accomplished.

REFERENCES

- [1] Aleksandr Reznik, Marcelo Godoy Simoes, Ahmed Al-Durra, and S. M. Muyeen. LCL Filter Design and Performance Analysis for Grid-Interconnected Systems. *IEEE Transactions on Industry Applications*, 50(2):1225–1232, 2014.
- [2] Kamran Jalili and Steffen Bernet. Design of LCL Filters of Active-Front-End Two-Level Voltage-Source Converters. *IEEE Transactions on Industrial Electronics*, 56(5):1674–1689, 2009.
- [3] Marwa Ben Said-Romdhane, Mohamed Wissem Naouar, Ilhem Slama Belkhodja, and Eric Monmasson. An Improved LCL Filter Design in Order to Ensure Stability without Damping and Despite Large Grid Impedance Variations. *Energies*, 10(3), 2017.
- [4] Carlos Gurrola-Corral, Juan Segundo, Miguel Esparza, and Roel Cruz. Optimal LCL-filter design method for grid-connected renewable energy sources. *International Journal of Electrical Power & Energy Systems*, 120, 2020.
- [5] Yong-Jung Kim and Hyosung Kim. Optimal design of LCL filter in grid-connected inverters. *IET Power Electronics*, 12(7):1774–1782, 2019.
- [6] Marco Liserre, Frede Blaabjerg, and Steffan Hansen. Design and control of an LCL-filter-based three-phase active rectifier. *IEEE Transactions on Industry Applications*, 41(5):1281–1291, 2005.
- [7] Grid code specifications, Fingrid, Finland. <https://www.fingrid.fi/en/grid/grid-connection-agreement-phases/grid-code-specifications/>, 2024. [Online; accessed March, 23, 2024].
- [8] IEEE Standard for Harmonic Control in Electric Power Systems. Standard IEEE 519-2022 (Revision of IEEE 519-2014), Institute of Electrical and Electronics Engineers, 2022.
- [9] IEEE Application Guide for IEEE Std 1547™-2018, IEEE Standard for Interconnection and Interoperability of Distributed Energy Resources with Associated Electric Power Systems Interfaces. Standard IEEE 1547.2-2023 (Revision of IEEE 1547.2-2008), Institute of Electrical and Electronics Engineers, 2024.
- [10] Electrical and electronic installations in ships – Electromagnetic compatibility (EMC) – Ships with a metallic hull. Standard IEC 60533:2015, International Electrotechnical Commission, 2015.

- [11] Uninterruptible power systems (UPS) – Part 2: Electromagnetic compatibility (EMC) requirements. Standard IEC 62040-2:2016, International Electrotechnical Commission, 2016.
- [12] Remus Narcis Beres, Xiongfei Wang, Frede Blaabjerg, Marco Liserre, and Claus Leth Bak. Optimal Design of High-Order Passive-Damped Filters for Grid-Connected Applications. *IEEE Transactions on Power Electronics*, 31(3):2083–2098, 2016.
- [13] M. Ben Saïd-Romdhane, M.W. Naouar, I. Slama. Belkhdja, and E. Monmasson. Simple and systematic LCL filter design for three-phase grid-connected power converters. *Mathematics and Computers in Simulation*, 130:181–193, 2016.
- [14] Miguel Esparza, Juan Segundo, Carlos Gurrola-Corral, Nancy Visairo-Cruz, Ernesto Barcenas, and Emilio Barocio. Parameter Estimation of a Grid-Connected VSC Using the Extended Harmonic Domain. *IEEE Transactions on Industrial Electronics*, 66(8):6044–6054, 2019.
- [15] Least Squares, The Mathworks Inc. <https://se.mathworks.com/help/optim/least-squares.html>, 2024. [Online; accessed July, 7, 2024].
- [16] Miguel Esparza and Juan Segundo-Ramirez. Optimal design of power electronics converters using the extended harmonic domain. In *2014 IEEE International Autumn Meeting on Power, Electronics and Computing (ROPEC)*, pages 1–6. IEEE, 2014.
- [17] Miguel Esparza, Juan Segundo, C. Nunez, Xiongfei Wang, and Frede Blaabjerg. A Comprehensive Design Approach of Power Electronic-Based Distributed Generation Units Focused on Power-Quality Improvement. *IEEE Transactions on Power Delivery*, 32(2):942–950, 2017.
- [18] Jesus J. Rico, Manuel Madrigal, and Enrique Acha. Dynamic harmonic evolution using the extended harmonic domain. *IEEE Transactions on Power Delivery*, 18(2):587–594, 2003.
- [19] D. Grahame Holmes and Thomas A. Lipo. *Pulse Width Modulation for Power Converters: Principles and Practice*, volume 18 of *IEEE Press Series on Power Engineering*, chapter Modulation of One Inverter Phase Leg, pages 95–152. John Wiley & Sons, 2003.
- [20] D. Grahame Holmes and Thomas A. Lipo. *Pulse Width Modulation for Power Converters: Principles and Practice*, volume 18 of *IEEE Press Series on Power Engi-*

- neering*, chapter Zero Space Vector Placement Modulation Strategies, pages 259–333. John Wiley & Sons, 2003.
- [21] D. Grahame Holmes and Thomas A. Lipo. *Pulse Width Modulation for Power Converters: Principles and Practice*, volume 18 of *IEEE Press Series on Power Engineering*, chapter Introduction to Power Electronic Converters, pages 1–55. John Wiley & Sons, 2003.
- [22] D. Grahame Holmes and Thomas A. Lipo. *Pulse Width Modulation for Power Converters: Principles and Practice*, volume 18 of *IEEE Press Series on Power Engineering*, chapter Modulation of Three-Phase Voltage Source Inverters, pages 215–257. John Wiley & Sons, 2003.
- [23] Alain Vande Wouwer, Philippe Saucez, and Carlos Vilas. *Simulation of ODE/PDE Models with MATLAB®, OCTAVE and SCILAB Scientific and Engineering Applications*, chapter An Introductory Tour, pages 1–44. Springer International Publishing, 2014.
- [24] Alain Vande Wouwer, Philippe Saucez, and Carlos Vilas. *Simulation of ODE/PDE Models with MATLAB®, OCTAVE and SCILAB Scientific and Engineering Applications*, chapter More on ODE Integration, pages 45–123. Springer International Publishing, 2014.
- [25] Choose an ODE Solver, The MathWorks, Inc. <https://se.mathworks.com/help/matlab/math/choose-an-ode-solver.html>, 2024. [Online; accessed October, 6, 2024].
- [26] The SciPy community. Solving initial value problems for ODE systems. <https://docs.scipy.org/doc/scipy/reference/integrate.html>, 2024. [Online; accessed October, 6, 2024].
- [27] Kendall Atkinson, Weimin Han, and David Stewart. *Numerical Solution of Ordinary Differential Equations*, chapter Taylor and Runge–Kutta methods, pages 67–93. John Wiley & Sons, Ltd, 2009.
- [28] Allan R. Hambley. *Electrical Engineering: Principles and Applications*, chapter Power in AC Circuits, pages 249–261. Pearson Education, 6th edition, 2011.
- [29] Rainer M. Storn and Kenneth V. Price. Differential Evolution - A Simple and Efficient Heuristic for global Optimization over Continuous Spaces. *Journal of Global Optimization*, 11(4):341–359, 1997.

- [30] Kenneth V. Price, Rainer M. Storn, and Jouni A. Lampinen. *Differential Evolution: A Practical Approach to Global Optimization*, chapter The Motivation for Differential Evolution, pages 1–34. Springer Berlin, Heidelberg, 1st edition, 2005.
- [31] Douglas C. Montgomery. *Design and Analysis of Experiments*, chapter Multiple Responses, pages 496–500. John Wiley & Sons Inc, 8th edition, 2013.

Appendix 1. Additional results from the experiments.

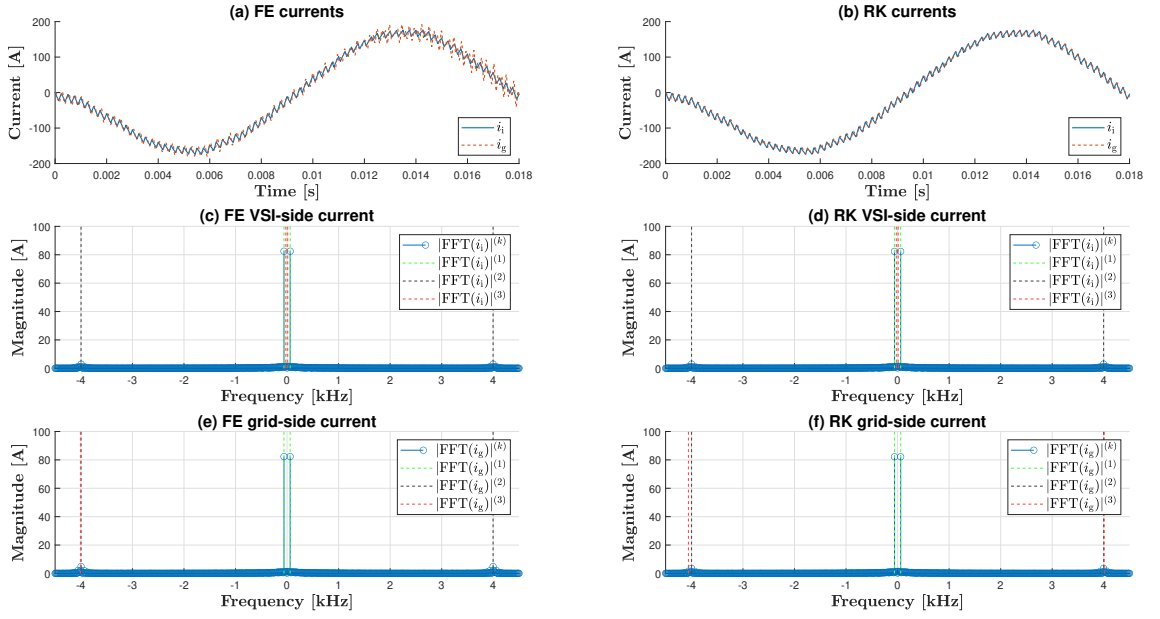


Figure A1.1. LCL ODE solutions: (a) Forward-Euler; (b) Fourth-order Runge-Kutta; (c) FE i_i FFT spectrum magnitudes; (d) RK i_i FFT spectrum magnitudes; (e) FE i_g FFT spectrum magnitudes; (f) RK i_g FFT spectrum magnitudes.

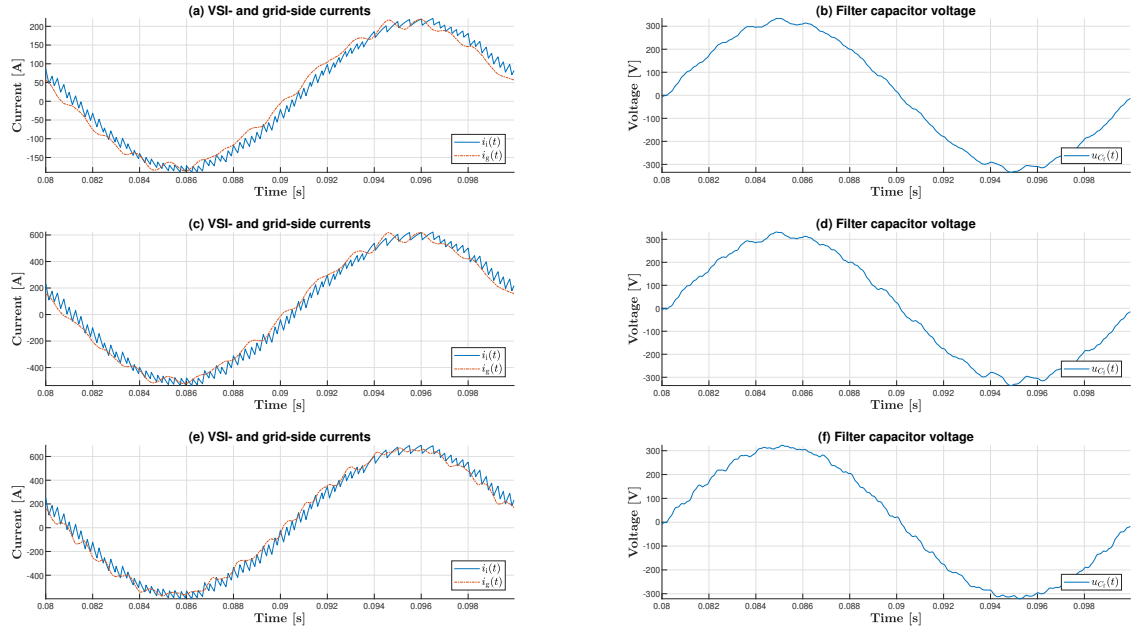


Figure A1.2. Top DE candidate solution for each generation size: (a) i_i and i_g , $N_g^{(i)} = 100$; (b) u_{C_f} , $N_g^{(i)} = 100$; (c) i_i and i_g , $N_g^{(i)} = 300$; (d) u_{C_f} , $N_g^{(i)} = 300$; (e) i_i and i_g , $N_g^{(i)} = 900$; (f) u_{C_f} , $N_g^{(i)} = 900$.

Appendix 1. (continued)

Table A1.1. Top three design parameter candidates for each maximum number of generations $N_g^{(i)}$, $i \in \{1, 2, 3\}$ as per unit values.

i	L_i [p.u.]	C_f [p.u.]	L_g [p.u.]
$N_g^{(1)} = 100$			
1.	0.715	0.129	0.040
2.	0.620	0.151	0.034
3.	0.738	0.090	0.012
$N_g^{(2)} = 300$			
1.	0.218	0.274	0.020
2.	0.218	0.274	0.020
3.	0.218	0.274	0.020
$N_g^{(3)} = 900$			
1.	0.182	0.274	0.008
2.	0.182	0.274	0.008
3.	0.182	0.273	0.008